TREE SPECIES CLASSIFICATION USING UAV-RGB IMAGES AND MACHINE LEARNING ALGORITHMS IN A MIXED TEMPERATE FOREST: A CASE STUDY OF HAAGSE BOS, NETHERLANDS

MERON AWOKE ESHETAE

[July, 2020]

SUPERVISORS:

Ir. L.M. Van Leeuwen- de Leeuw (First Supervisor)
Dr. Y.A. Hussin (Second Supervisor)

TREE SPECIES CLASSIFICATION USING UAV-RGB IMAGES AND MACHINE LEARNING ALGORITHMS IN A MIXED TEMPERATE FOREST: A CASE STUDY OF HAAGSE BOS, NETHERLANDS

MERON AWOKE ESHETAE
Enschede, The Netherlands, July, 2020

Thesis submitted to the Faculty of Geo-Information Science and Earth Observation of the University of Twente in partial fulfilment of the requirements for the degree of Master of Science in Geo-information Science and Earth Observation.
Specialization: Natural Resource Management

SUPERVISORS:
Ir. L.M. Van Leeuwen- de Leeuw (First Supervisor)
Dr. Y.A. Hussin (Second Supervisor)

THESIS ASSESSMENT BOARD:
Dr. L.L.J.M. Willemen (Chair)
Dr. Tuomo Kauranne (External Examiner, Lappeenranta University of Technology , Finland)

ABSTRACT

Acquiring reliable and accurate information on tree species is of great importance for effective forest monitoring including assessing biodiversity and ecosystem services, building resilience to climate change, and conserving endangered or critical tree species. In view of this, this study aimed at classifying and mapping tree species using UAV-RGB images and machine learning algorithms in a mixed temperate forest, Haagse Bos, Netherlands. For this purpose, the UAV-RGB images captured in September 2019 (leaf-on season) and February 2020 (leaf-off season) were used. A combination of leaf-on and leaf-off season UAV-RGB images were also applied to classify tree species. The object-based image analysis in conjunction with the Support Vector Machine (SVM), K-nearest neighbour (KNN) and Random Forest (RF) classifiers were used to separate seven tree species, three from the broadleaved and four from the coniferous ones. The UAV-RGB image captured in the leaf-on season were used to compare all the three classifiers, and to assess the tree crown segmentation accuracy in the young and mature mixed forest stands using a single Orthophoto and combinations of canopy height model (CHM) and Orthophoto. The accuracy of the multi-resolution segmentation (MRS) algorithm in segmenting tree crown was assessed using three evaluation performance metrics: over segmentation, under segmentation and total segmentation error. Regarding the tree species classification, comparison of classifiers were made based on the overall accuracy and kappa coefficient which were determined from the confusion matrix developed from the 5-fold cross validation. The best classifier was subsequently applied in the leaf-off and combinations of seasons of UAV-RGB images for classifying tree species.

Results showed that a single Orthophoto and combinations of Orthophoto and CHM in mature (young) forest stands produced an overall segmentation accuracy of 82 % (73%) and 83% (76%), respectively. The UAV-derived CHM improved the tree crown segmentation of young forest stand by 3%, but it slightly reduced the segmentation accuracy of the mature forest stand by 1%. Among the classifiers, the SVM classifier outperformed the RF and KNN and produced an overall accuracy of 78.94% and a kappa coefficient of 0.75. All the classifiers except KNN produced low values of producer and user accuracies for classifying all coniferous tree species as compared to the broadleaved tree species. The combinations of UAV-RGB images improved the leaf-on and leaf-off season tree species classification by 3.7% and by 11.3 %, respectively. Overall, applying cost-effective UAV-RGB images acquired at different seasons improves the tree species classification in a mixed temperate forest as compared to using a single season UAV-RGB image. This study suggests to use SVM classifier in the study area to classify tree species for assessing the above ground biomass at species level and for utilizing the natural resource in sustainable manner.

Keywords: UAV-RGB image; Leaf-on season; Leaf-off season; object-based image analysis; Machine learning algorithms; Haagse Bos

ACKNOWLEDGEMENTS

First, and for most, I would like to thank my holy father, God, for his support, care and endless love during all my works and stay in this beautiful country, the Netherlands.

I would like to acknowledge to my supervisor Louise for her valuable advice, encouragement and critical comment during the research period. Louise, I have learned a lot from you. Your guidance and the question you raised starting from the proposal writing to completion of this thesis work would help me to know the subject matter very well and also to improve my writing skills. Thank you again. My gratitude also goes to my second supervisor, Dr Yousif, for his encouragement and constructive comments. Even in the difficult time we spent together in Thailand where this research work was planned, your support was unforgettable, thank you, Dr Yousif. I would like to thank my Husband, Kirubel Mekonen, my family and friends for their endless love and care.

I would like to extend my sincere appreciation to my employer for giving me leave of absence during my study at the University of Twente, ITC, and the Netherlands Fellowship program for sponsoring my studies. I thank my entire coursemates, NRS 2019/2020 batch, for all challenges, knowledge sharing and happy time we spent together at ITC, Enschede, Netherlands.

TABLE OF CONTENTS

LIST OF FIGURES

LIST OF TABLES

LIST OF ACRONYMS

CART	Classification and Regression Trees
CHM	Canopy height model
DT	Decision tree
DSM	Digital surface model
DTM	Digital terrain model
ESP	Estimation of Scale Parameter
GCP	Ground control point
GPS	Global Positioning System
GLCM	Gray-Level Co-occurrence Matrix
KNN	K-nearest neighbour
LiDAR	Light detection and ranging
MLC	Maximum Likelihood classifier
MDA	Mean Decrease Accuracy
MDG	Mean Decrease Gini
MRS	Multi-Resolution Segmentation
OA	Overall Accuracy
OBIA	Object-based image analysis
OOB	Out-of-bag
PA	Producer Accuracy
RANSAC	Random Sample Consensus
RBF	Radial kernel basis function
REDD	Reducing Emissions from Deforestation and Forest Degradation
RF	Random forest
RMS	Root Mean Square Error
RTK GNSS	Real-Time Kinematic Global Navigation Satellite System
SVM	Support Vector Machine
SFM	Structure for motion
UAV	Unmanned Arial vehicle
UA	User accuracy

1. INTRODUCTION

1.1. Background

Forest plays a significant role in providing ecosystem, social, and economic services. It protects biodiversity by providing nursing and breeding for different plant and animal species, preventing the effect of erosion and floods through their rooting system. Forests also sequester carbon by capturing carbon dioxide from the atmosphere and contribute a lot to reduction of carbon emissions and to combating climate change (Bonan, 2008). Nowadays, forests cover approximately 30% of the land surface in temperate and boreal regions and 42 million km² in tropical lands of the earth surface. In Europe, forest covers more than 40% of the land surface (Eurostat, 2018) and comprises different tree species grouped under the coniferous and broadleaved types.

Acquiring reliable and accurate information on tree species is of great importance for effective forest monitoring including assessing biodiversity and ecosystem services, building resilience to climate change, and conserving endangered or critical tree species (Wietecha et al., 2019). Such information gives insight for decision-makers to develop and implement appropriate policies and strategies for protecting forest biodiversity (Barredo José et al., 2015) and for Reducing Emissions from Deforestation and Forest Degradation (REDD+). Tree species information can be acquired during field inventories. However, this requires a high cost and a lot of human resources. Furthermore, the lack of accessibility in some forest areas makes the field investigation more challenging (Modzelewska et al., 2020). Currently, remote sensing has become an essential source of information for mapping individual tree species. Compared to the conventional field measurements, data acquired from satellite imagery can provide real-time and cost-effective information (Thomas et al., 2018).

Many researchers have been using different satellite imageries and classifiers to map tree species in different geographic and climatic regions. For example, Kovacs et al. (2010) used IKONOS sensor and unsupervised classifier to separate tree species in Guinea, West Africa, and their results showed that the unsupervised classifier shows a good result in classifying four tree species with an accuracy of more than 78%. Viennois et al. (2016) used Ikonos, GeoEye, QuickBird, and WorldView-2 sensors in conjunction with Maximum likelihood classifier to discriminate three tree species in Bali, Indonesia and their results revealed that tree species were more easily discriminated by imagery acquired from WorldView-2 sensors than other sensors. This is mainly associated with the spatial resolution of the sensors. In addition, they found an accuracy of 66%-80% from these satellite imageries. Wang et al. (2018) employed pixel-based and object-based classification approaches to differentiate five tree species in Dongzhaigang, China, using Pleiades-1 sensor

combined with random forest classifier. They reported that the machine learning algorithms used in the object-based image analysis showed a better accuracy result (78%) in classifying tree species than pixel-based image analysis. In general, relative to the spatial resolution of the unmanned aerial vehicles (UAV), the aforementioned researchers used a low spatial resolution satellite imagery in their studies, which might affect the tree classification accuracy result.

UAV based tree species classification and mapping have recently received more attention from the scientific communities. This is mainly due to the fact that UAV has a potential to capture high-resolution data, and its flexibility to acquire data within a short time, and its low operational costs (Otero et al., 2018). Several UAV studies have used multi-resolution segmentation (Xie et al., 2019) and simple linear iterative clustering (Effiom et al., 2019) approaches in conjunction with supervised and machine learning algorithms to classify individual tree species. They attempted to extract object feature variables such as spectral, spatial and tree height, from the segmented image to classify tree species. For example, Xie et al. (2019) and Cao et al. (2018) applied multi-resolution for segmentation of a UAV hyperspectral image along with Maximum Likelihood classifier (MLC), and machine learning classifiers including Classification and Regression Trees (CART), Support Vector Machine (SVM), K-nearest neighbour (KNN) and Random forest (RF) so as to identify tree species in China. The authors found that machine learning algorithms outperformed the supervised classifiers (MLC) to differentiate tree species from other land cover classes. The MLC cannot fully exploit the texture and tree height variables obtained from the high spatial resolution imagery, but its performance is better using spectral (band) features only. They conclude that machine learning algorithms and multiple source data improved tree species classification. Heinzel and Koch (2012) also used UAV data and SVM classifier to differentiate four temperate tree species (Pine (*Pinus sylvestris*), Spruce (*Picea abies*), Oak (*Quercus petraea*) and Beech (*Fagus sylvatica*). They found a good classification accuracy result, 83.1%-90.7% using the machine learning algorithms as well.

In addition to the machine learning algorithms and different features such as spectral, texture and tree height variables, satellite images captured at different seasons improve the tree species classification by providing information on the phenological properties of a tree. Specifically, in a temperate forest, some of the tree species change their leaf colours, and their leaf drops in autumn and they expand their leaf in the spring. These changes considerably affect the tree species classification results as the tree species are showing different spectral reflectance in those seasons (Delpierre et al., 2016; Grabska et al., 2019; Madonsela et al., 2017; Persson et al., 2018). In view of this, Natesan et al. (2019) classified tree species using UAV-RGB images captured in different seasons in combination with deep learning algorithms. They reported that multi-temporal images outperformed a single season spectral image in discriminating tree species. Xie et al. (2019) and Hill et al. (2010) found a similar result by using different satellite imageries and classifiers. Wessel et al. (2018) and Persson et al. (2018) also used multi-temporal Sentinel-2 imagery and two machine learning (SVM and RF) algorithms to classify coniferous and broadleaved tree in two forest areas of Germany, and

Sweden, respectively and they also found that the multi-temporal image improves tree species classifications compared to a single season image.

1.2. Problem statement

Tree species mapping can be employed using field survey, manual interpretation of aerial photographs, and remote sensing techniques. The first two conventional approaches are time-consuming, laborious, and costly with limited spatial and temporal sampling (Modzelewska et al., 2020). In contrary, remote sensing approaches provide reliable and timely information on tree species at the required spatial and temporal scales.

Remote sensing plays a vital role in classifying tree species for effective forest assessment and monitoring. However, the accuracy of tree species classification is highly affected by the spatial resolution of remotely sensed imageries, the applied segmentation methods, choice of the classifiers, seasons and feature variables considered for image classification. These resulted in uncertainties in the classification accuracy result. In this regard, object-based image analysis (OBIA) in high spatial resolution satellite imagery believed to improve the classification accuracy results (Cao et al., 2018; Modzelewska et al., 2020). In addition to this, remotely sensed imagery acquired in different seasons could also improve tree species classification as the tree species are showing different spectral reflectance for different seasonal images, which is used to discriminate tree species (Persson et al., 2018; Wessel et al., 2018). Specifically, in a temperate forest, the spectral signature of broadleaved tree species become different, when these species are colourful in autumn (leaf-on season), drop their leaf in winter (leaf-off season), and they bloom in the summer season. However, studies on the application of cost-effective UAV-RGB images for classifying tree species in a temperate forest under the leaf-on and leaf-off conditions are limited. Moreover, a comparison of a single date and a combination of two seasonal UAV-RGB images in classifying tree species found in a mixed broadleaved and coniferous forest stand has rarely been explored. This understanding benefits the biodiversity, above ground biomass estimation, and ecosystem service studies.

Even though multiple source data (e.g. spectral, spatial and tree height (CHM) variables), as input for different classifiers, considerably improved the classification accuracy result (Cao et al., 2018), selection of appropriate classifier is still a challenging issue in a remote sensing based tree species classification. Several studies often used KNN, RF and SVM algorithms to discriminate tree species in temperate and tropical forests (e.g. Xie et al., 2019; Cao et al., 2018; Modzelewska et al., 2020; Pham et al., 2019). However, the performance of these classifiers varies from region to region and from species to species, and thus must be assessed on a local basis. Furthermore, little information has been documented on the accuracy of these classifiers to differentiate tree species in a mixed temperate forest using UAV-RGB image.

1.3. Research objectives

1.3.1. General objectives

The general objective of this study is to classify and map tree species using UAV-RGB images, and machine learning algorithms such as SVM, RF and KNN.

1.3.2. Specific objectives

The specific objectives of this study are to:

1. assess the segmentation accuracy in mature and young forest stands using a single Orthophoto and a combination of CHM and Orthophoto,

2. assess the performance of machine learning classifiers to differentiate tree species using the leaf-on season UAV-RGB image,

3. examine the accuracy of tree species classification using the leaf-on and leaf-off season UAV-RGB images and compare the results, and

4. assess the combined effect of leaf-on and leaf-off season UAV-RGB images on tree species classification.

1.3.3.   Research question

1. How accurately can the tree crowns be delineated by multi-resolution segmentation? Does a combination of UAV derived CHM and Orthophoto improve the segmentation accuracy result in mature and young forest stands?

2. Which classifiers (SVM, RF and KNN) perform best in differentiating tree species using September 2019 UAV-RGB image (leaf-on season)?

3. How accurate are tree classification results obtained from leaf-on and leaf-off season UAV-RGB images?

4. Does the tree species classification accuracy result improve when the combinations of leaf-on and leaf-off season UAV-RGB images are used?

5. Which UAV-RGB image (leaf-on, leaf-off, and/or combinations) yields best tree species classification result?

1.3.4.   Research hypothesis

Q1: Ho: A combination of Orthophoto and CHM does not improve the tree crown segmentation result in mature forest stand

Ha: A combination of Orthophoto and CHM improves the tree crown segmentation result in mature forest stand

Ho: A combination of Orthophoto and CHM does not improve the tree crown segmentation result in young forest stand

Ha: A combination of Orthophoto and CHM improves the tree crown segmentation result in young forest stand

Q2: Ho: RF outperforms SVM in classifying tree species using leaf-on season UAV-RGB image

Ha: SVM outperforms RF in classifying tree species using leaf-on season UAV-RGB image

Q4: Ho: The combinations of leaf-on and leaf-off season UAV-RGB images does not improve the tree species classification result compared to a single season spectral image.

Ha: The combinations of leaf-on and leaf-off season UAV-RGB images improve the tree species classification result compared to a single season UAV-RGB image

2. LITERATURE REVIEW

2.1. Pixel-based and object-based image analysis in classifying tree species

A pixel-based and object-based approaches are the two most widely applied technique in remote sensing-based tree species classification. Several studies have been undertaken to compare these two approaches by using different classifiers and satellite imageries. The results of these studies are reviewed and given as follows;

Using SPOT-5 HRG imagery, Duro et al. (2012) evaluated pixel-based and object-based approaches for classifying land cover classes using three machine learning algorithms: SVM, RF and Decision Tree (DT). Their results revealed that pixel-based and object-based image analysis showed insignificant difference when the same machine learning algorithms were applied for these approaches. In contrast, other studies showed that object-based image analysis (OBIA) outperformed pixel-based image analysis in classifying land cover classes in high spatial resolution of remotely sensed imageries (e.g. Yan et al., 2006; Yu et al., 2006; Platt & Rapoza, 2008 ; Myint et al., 2011). For example, Yan et al. (2006) used Terra Advanced Spaceborne Thermal Emission and Reflection Radiometer (ASTER) imagery in conjunction with MLC and KNN classifier for pixel-based and object-based image analysis, respectively. They found an overall classification accuracy result of 83% and 46% from the object-based and pixel-based image analysis, respectively. Similarly, Yu et al., (2006) applied the same machine learning algorithms in object-based and pixel-based image analysis to classify land cover classes from a high resolution airborne imagery, and their results showed that object-based image classification considerably outperformed pixel-based classification by 17%. Using Multispectral IKNOS images, Platt and Rapoza (2008) compared pixel-based and object-based approaches by applying KNN and MLC algorithms. Their results showed that object-based KNN classification had a better performance result (78%) than a pixel-based MLC classification (64%). Myint et al., (2011) have also attempted to compare pixel-based MLC classification and object-based KNN classification to classify urban land covers using Quickbird imagery. They reported that object-based classification (90%) showed the highest accuracy result as compared the pixel-based (67%). In general, as compared to OBIA, the classification accuracy results obtained from a pixel-based approach is poor for high spatial resolution imagery because of the "salt-and-pepper" effects associated with pixel-based image analysis. Because of these reasons, this study was used object-based image analysis in classifying tree species using different machine learning algorithms.

Object-based image analysis (OBIA) has become increasingly applied to analysis of high spatial resolution imagery over the last ten years (Blaschke et al., 2008). In OBIA, image segmentation is an important step and a prerequisite as the accuracy of the classification results mainly depends on the accuracy of the segmentation (Mountrakis et al., 2011; Su & Zhang, 2017). Three different image segmentation methods

have been widely applied in different fields. These methods are Edge-based segmentation (Y. Lu & Jain, 1989; Zhou et al., 1989), Region-based segmentation (Ohta et al., 1980; Pal & Pal, 1987; Pong et al., 1984), Hybrid Method (Fan et al., 2001). In edge-based segmentation, the boundaries/edge of object are identified first and then the detected boundaries/edges transformed into closed boundaries using different algorithms. In contrast, region-based segmentation uses the opposite approach, and it starts from the inside of an object and increases until the boundaries of the object meet (Zhang et al., 2018). To overcome the limitation of the Region and Edge-based segmentation, some of the researchers use hybrid segmentation methods. The reader can refer to (Hossain & Chen, 2019) for further information about the pros and cons of the mentioned segmentation methods.

In this section, the Multi-Resolution Segmentation (MRS) method, one of the most widely applied methods in the literature, are reviewed. Basically, this segmentation method is categorized under region-based segmentation methods. The premise of MRS is to segment images to object images based on the scale, shape and compactness parameters. The key challenges of this method is setting appropriate parameters to define the object segments. Among the mentioned parameters, selecting a suitable scale takes the lion share. To optimize this parameter, several studies have been used different approaches: Genetic algorithms (Saba et al., 2016); fuzzy logic and iterative optimization (Esch et al., 2008); Statistical Region Merging and Minimum Heterogeneity Rule (Li et al., 2008) and integrated graph-based segmentation (Gu et al., 2018). Some studies also used supervise and unsupervised methods to select optimal parameters. Under the supervised methods, several authors applied trial and error methods to optimize parameters by comparing segmentation results obtained from the MRS and the manually delineated ones (Ghosh & Joshi, 2014; Wang et al., 2018). Comparison/evaluation of segmentation result were then employed by computing the overlap area (Clinton et al., 2010) and by correctly matching the number of objects (Liu & Wang, 2014). In contrast, in the unsupervised methods, intra-segment homogeneity and inter-segment heterogeneity were estimated using estimation of scale parameters (ESP) tool and then the optimized parameters were selected (Drǎguţ et al., 2014; Zhang et al., 2008).

2.2. High spatial resolution remotely sensed imagery and machine learning algorithms for tree species classification

Acquiring accurate and reliable classification of individual tree species from the remotely sensed imageries remains challenging because of different factors such as the spatial resolution of the data source, the choice of the classifiers, selection of features variable (spectral, spatial and temporal) used for classification, and similar spectral characteristics of the species. In this regard, the classifiers, sensors and feature variables used by the previous studies for classifying tree species are summarized in Table 1. Using a single season spectral image and combinations of bands from different seasons, numerous studies were undertaken to classify tree species, and their major finding are presented as follows;

Using a single season spectral image, Zhang et al. (2018) attempted to discriminate four mangrove species in Hong Kong using WorldView-2 and radar data in combination with rotation of forest (Rof) classifiers.

Their results showed that multi source data (spectral, texture and tree height) improves the tree species classification accuracy result instead of applying the spectral bands alone. Cao et al. (2018) tried to classify six mangrove species in Oiao Island, China, using UAV imagery and two machine learning algorithms, SVM and KNN. The performance of these classifiers were also evaluated by applying the spectral, texture and tree height information. They used UAV data, and digital surface model (DSM) generated from UAV imagery to delineate the tree crowns using MRS. The segmentation parameters were optimized by trial and error, and they found a good segmentation accuracy results. Moreover, their study results revealed that the classification result obtained from the machine learning algorithms were much improved when combining the spectral, texture and tree height variables instead of using a single variable.

Table 1: Summary of machine learning algorithms and high spatial resolution satellite imageries used for tree species classification.

Classifier	Sensor	Features variables used for classification	Identified Species	Season	Reference
Rotation of Forest	WorldView-3 and Radarsat-2	Spectral and texture	Four mangrove species: *Kandelia obovate*, *Avicennia marina*, *Acanthus ilicifolius* and *Aegiceras corniculatum*	SS	Zhang et al., 2018
SVM, KNN	UAV hyperspectral images	Spectral, texture and tree height	Six Mangrove species	SS	Cao et al., 2018
DT	LiDAR	Spectral	White Birch Sugar mapleAspenJack pineWhite Pine	SS	Hu, 2012
NDVI	UAV-Hyperspectral	Spectral	Beach, Fir and Spruce	SS	Brovkina et al., 2018
Tree-Crown Object	UAV- RGB	Spectral	Metasequoia, Platanus ,Platanus and Camphora	SS	Feng & Li, 2019
SVM and RF	Sentinel 2	Spectral	Oak and Beech	SS and CS	Wessel et al., 2018
RF	Sentinel 2	Spectral	Norway spruce, Scots pine, Hybrid Larch, Birch and Pedunculate Oak	SS and CS	Persson et al., 2018
MLC, RF, SVM, KNN and Decision Tree(DT), ANN	ZiYuan-3 multispectral and stereo images	Spectral, texture and tree height	Larch, Chinese Pine, Mongolia Scotch pine, red Pine, Birch, aspen, Andelm	SS and CS	Xie et al., 2019

SS stands for single season spectral image; CS stands for the combination of two or more seasons(multi-temporal) of spectral image.

In addition to the classification of the coniferous species, previous studies have also been attempted to classify deciduous tree species using high spatial resolution imagery and machine learning algorithms. On one hand, these studies used a single season spectral image. On the other hand, they applied multi-temporal datasets to classify deciduous and coniferous tree species (Table 1). Using a single season spectral image, Hu, (2012) applied light detection and ranging (LiDAR) data and decision tree algorithms to classify mature coniferous and deciduous trees in the complex Canadian forest. The individual tree crown were delineated using multi-scale crown delineation segmentation approaches, and their results showed that LiDAR were effective to identify mature deciduous and coniferous tree species. Tree species classification using UAV-RGB images captured on a single have also been undertaken (Feng & Li, 2019) and their results show that the applicability of UAV-RGB image in classifying tree species was promising. Wessel et al. (2018) used Sentinel-2 imagery and two machine learning (SVM and RF) algorithms to classify deciduous and broadleaved tree in two forest areas of Germany. Their results showed that applying multi-temporal datasets improve the classification accuracy results for both classifiers and the SVM classifiers outperformed RF using this dataset. Persson et al. (2018) also attempted to classify mature coniferous and deciduous tree species in central Sweden forest using multi-temporal (spring, summer and fall) Sentinel-2 in combined with the RF classifier. Their result showed that the combination of all bands from all seasons considerably improved the classification accuracy result (97%) compared to a single season spectral image. Compared to summer and fall seasons, the spring season gave a better classification result (80%) in classifying coniferous and deciduous species. Overall, they conclude that multi-temporal satellite imagery improves the tree species classification as the tree species are showing different spectral signature for different seasons.

Xie et al. (2019) have also applied multi-temporal multispectral and stereo images to classify tree species in China. They used spectral bands and textures variable, canopy height, slope and elevation from the stereo images as input to MLC, KNN, SVM, RF and DT classifiers. Tree species classification substantially improved by 6% to 12% while applying a combination of leaf-on and leaf-off seasons. In addition, the SVM and RF outperformed the remaining classifiers. Overall, the results of the aforementioned studies (Table 1) showed that the tree species classification accuracy results, particularly for deciduous and coniferous tree species, improved while applying combinations of all bands from different seasons. However, there is a research gap on the application of cost effective UAV-RGB image in classifying tree species a mixed temperate forest under the leaf-on and leaf-off conditions.

3. MATERIAL AND METHOD

3.1. Description of the study area

This study was undertaken in Haagse Bos, one of the oldest forest in the Netherlands. It is geographically located between 476500m N to 477700m N and 261000m E to 262000 m E (Figure1) and found approximately 8km away from the centre of Enschede, Netherlands. Haagse Bos forest is currently managed by the private company and mainly provides environmental, economic, social, and ecosystem services. This forest has covered a total area of 43 ha. The forest consists of mature and young mixed broadleaved and coniferous species: Scot Pine (*Pinus Sylvestris*), Douglus Fir(*Pseudotsuga menziesii*), Norway Spruce(*Picea abies*), European Larch(*Larix Decidua*), European Beech(*Fagus sylvatica*), Oak (*Quercus robur*), European white birch (*Betula pendula*) and Alder (Figure1). The broadleaved tree species are dominant in the study area. Based on tree crown projection area and ages of trees, the study area is divided into two forest stands: mature mixed broadleaved and coniferous tree (Figure 1: polygon outlined with red colour) and young mixed broadleaved and coniferous tree (Figure 1: polygon outlined with yellow colour) and there area coverage is 24 and 2.4 Ha respectively.

The study area received a total annual rainfall of 841mm. The highest rainfall is recorded in the month of November, which accounts for 10% of the total annual rainfall. The average annual maximum and minimum temperature of the study area is 13.5^0C and 6.6^0C, respectively. The warmest month is August whereas the coldest one in February.
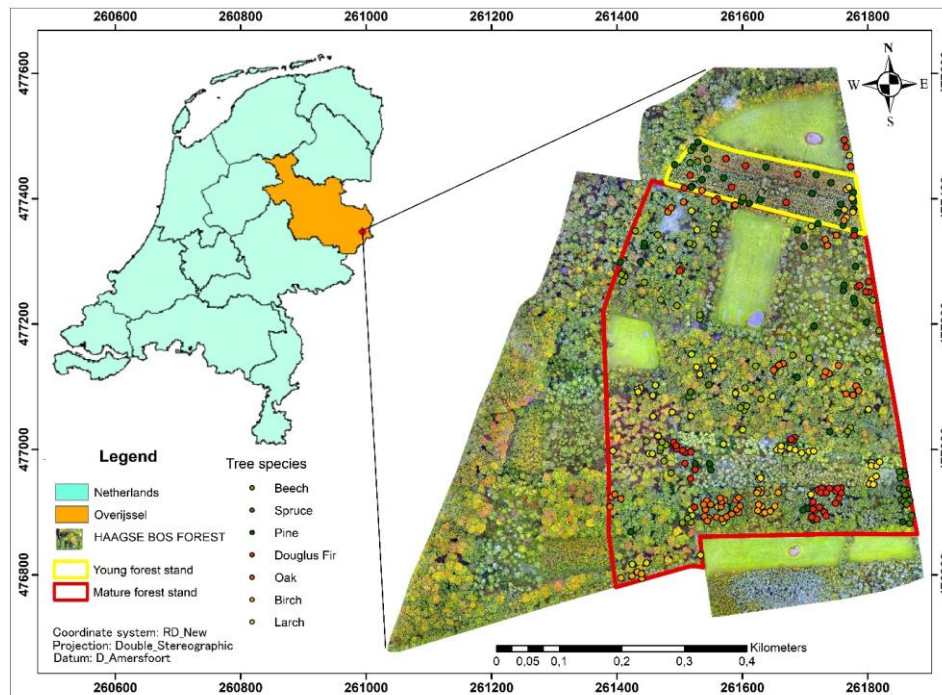
Figure 1: Location map of the study area along with the spatial distribution of the tree species in mature and young mixed broadleaved and coniferous forest stands.

3.2.   Datasets

The datasets used in this study include UAV-RGB images acquired in September 2019 and February 2020 and field survey data. Moreover, Google earth image was also used to assist the data collection. The list of equipment used for collecting the primary data is presented in Table2. Similarly, the following software were used for processing and analyzing the collected data;

- ArcGIS 10.6.1 for spatial data analysis and mapping,
- eCognition 9.2.1 developer for image segmentation and object features extraction,
- Pix4D for Photogrammetry pre-processing including DSM and DTM creation,
- Cloud compare for 3-D point cloud visualization,
- R statistical packages for implementing machine learning algorithms for tree species classification.

Table 2: List of field equipment used in this study.

Equipment	Purpose
Digital camera	Taking pictures of trees and others related information
Handheld Garmin GPS	Locating tree species
Field datasheet and pencil	Data recording
GNSS RTK	Collect ground control points(GCPs)
Ground control point (GCP) markers	Mark GCPs

3.3.   Methods

The methodology applied in this study comprises five major parts: (1) UAV data acquisition and field survey; (2) Photogrammetric image pre-processing; (3) Image processing including generation of Orthophoto, Digital Surface Model (DSM) and Digital Terrain Model (DTM) from the 3D point clouds; (4) Object-based image analysis includes image segmentation, feature extraction, and classification; and (5) accuracy assessment of segmentation and tree species classification. The detailed description of each part is presented in subsequent sections. The overall workflow of the study is shown in Figure 2.
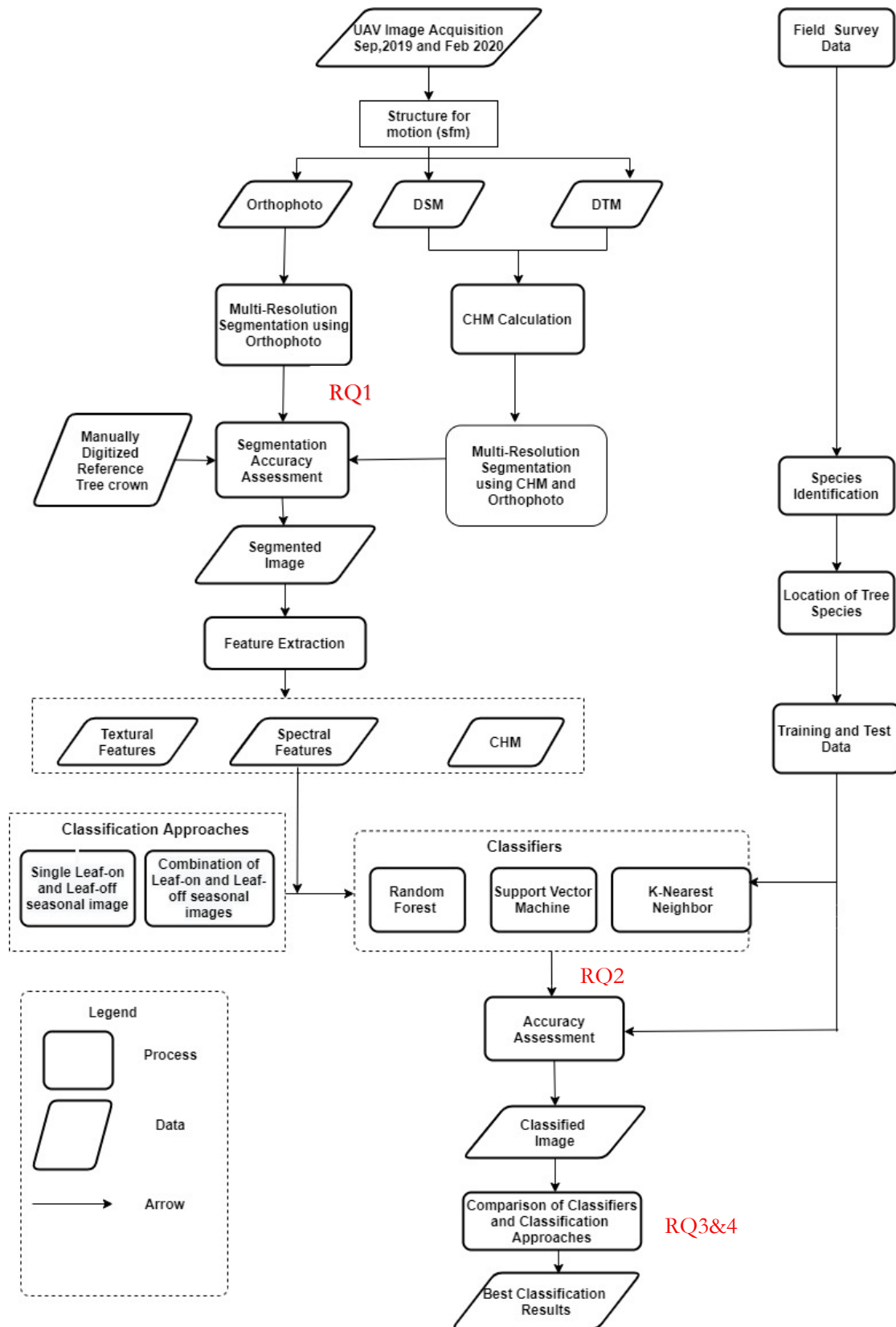
Figure 2: Workflow of the study.

3.3.1. Field Data Collection

The field survey was conducted in the study area from the end of February to mid-March, 2020. The GPS coordinates of tree species from the young and mature mixed coniferous and broadleaved forest stands were collected. In this study, a combination of purposive and random sampling techniques were applied to collect the data. Purposive sampling were employed to collect tree locations data from a homogeneous cluster of the same species. Efforts were also made to randomly collect the location of individual tree species in areas where a homogeneous clustering of a tree is missing. Moreover, the GPS coordinates of other land cover types such as open area, water and road, were also collected and categorized as non-tree area. As a result, a total of 293 sample coordinates of which 252 sample coordinates from the mature forest stand and 41 from the young forest stand were collected (Table 3).

About eight tree species were identified during the field survey: Scot Pine, Douglas Fir, Norway Spruce, European Larch, European Beech, Oak, European white Birch and Alder. The first four species are coniferous trees, and the remaining are the broadleaved ones. The broadleaved tree species are the dominant trees in the study area. The distribution of the number of ground truth data collected in the young and mature forest stand is presented in Table 3. Since the number of Alder species trees in the study area is very small (Table 3), this species was excluded in tree species classification. Moreover, we have also excluded the young forest stand because all the identified tree species are not existed in this forest stand and the sample size of the classes is too low for tree species classification. Because of this reason, the tree species classification were undertaken in the mature mixed forest stand alone. To this end, about 247 tress sample, excluding Alder, were used for tree species classification (Table3). However, it is very important to note that the tree crown segmentation accuracy assessment were performed in both the young and mature forest stands.

Table 3:Distribution of the number of ground truth data in the young and mature forest stands.

Category	Tree species	Distribution of tree species(No.)		Total
		Young forest stand	Mature forest stand	
Coniferous	Scot pine	7	22	29
	Douglas Fir	-	41	41
	Norway Spruce	4	29	33
	European Larch	8	18	26
Broadleaved	Oak	5	44	51
	European White Birch	9	17	26
	European Beech	8	40	48
	Alder	-	5	5
Non –tree area		-	36	36
Total		**41**	**252**	**293**

3.3.2. UAV Image Acquisition

Two UAV-RGB images acquired in September 2019 and February 2020 were used to classify tree species under the leaf-on and leaf-off conditions. In this study, September 2019 and February 2020 UAV images represent autumn (leaf-on) season and winter (leaf-off) seasons, respectively. These seasonal classifications were made based on the leaf-phenological stages of the broadleaved tree species, which are colourful in autumn (the leaf-on season) and tend to drop their leaves in winter (leaf-off season). Moreover, a combination of leaf-on and leaf-off season UAV-RGB images, a combination of all the bands (6 in number) of the two seasons UAV-RGB image, were also used to classify tree species. The UAV-RGB image that was lately captured in May 2020 also used to support the discussion parts of this study but not used for tree species classification. In order to ensure consistent comparisons between the three UAV-RGB images captured at different seasons, efforts were made to apply the same UAV flight height, flight pattern, overlap areas and angle of the camera as presented in Table 4. However, we found different the spatial resolution for September 2019 (4.6cm) and February 2020 (4.9cm) images. To match these resolutions, the spatial resolution of September 2019 image were up-scaled from 4.6 cm to 4.9cm using nearest neighbour resampling method, one of the most widely resampling method that preserve the spectral properties of a pixel.

Table 4: UAV flight parameters and their corresponding values.

UAV flight Parameters	Value
Flight Pattern	Double grid
The angle of the camera(Phantom4)	80 degree
Speed	Slow
Front Overlap	90%
Side Overlap	80%
Flight Height	120m
Spatial resolution (pixel size)	4.6cm for Sep, 4.9cm for Feb, and 4.58cm for May images.

3.3.3. UAV Data Processing and Generation of Orthophoto, DSM and DTM

The UAV data were processed using Pix4D software by applying a technique called structure for motion (SFM), a photogrammetric process of establishing a three-dimensional scene from a set of multiple overlapping two dimensional UAV images. In these processes, the position of the camera and the geometry of the scene were established simultaneously by automatically identifying matching features in multiple images. Random Sample Consensus (RANSAC) algorithms were used to match these features (Fischler & Bolles, 1981). Taking a minimum of two tie-points in three images, 3-D point clouds having a relative

coordinate system were generated, and their coordinates were transformed into real-world (absolute) coordinate system. For the absolute orientation of 3-D point clouds, about six ground control points (GCP) were collected using Real-Time Kinematic Global Navigation Satellite System (RTK GNSS), and three GCPs were used for the checkpoint. The quality report result revealed that the Root Mean Square error (RMSE) error of 0 m (Figure3) and 0.001 (Annex1) were reported for September 2019 and February 2020 UAV-RGB images, respectively. These results are close to 0 and acceptable for transforming the relative coordinates of the 3D point clouds to real-world coordinates.
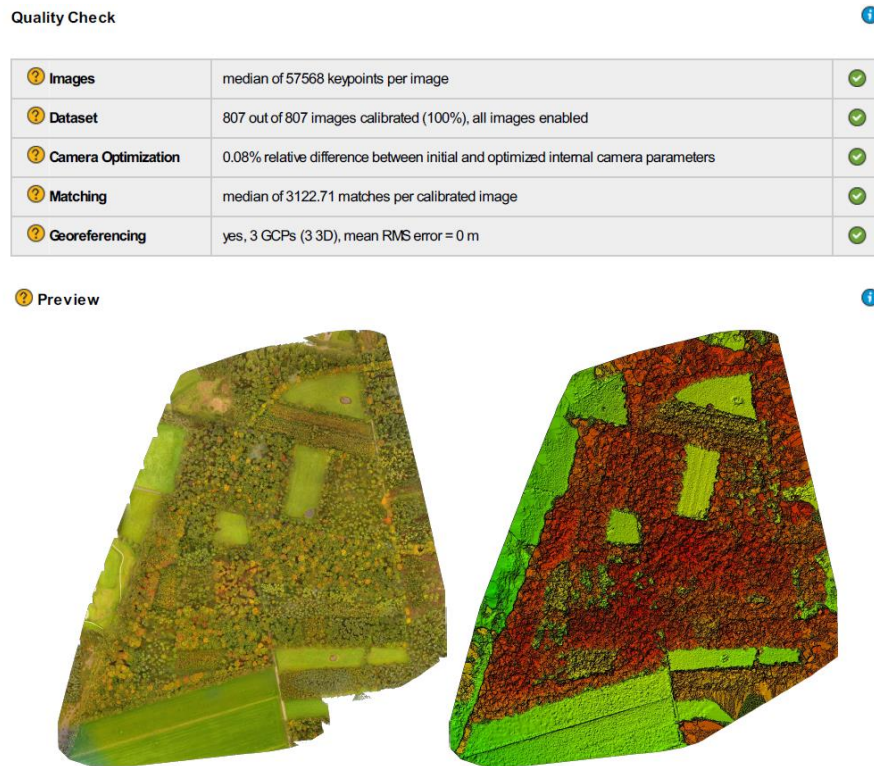
Figure 3: A quality report generated by Pix4D mapper for UAV data processing of September 2019 UAV-RGB image.

3.3.4.   Calculation of CHM

Once the dense point clouds were constructed through aerial triangulation, Digital surface Model (DSM), Digital Terrain Model (DTM) and Orthophoto were generated. Using the generated DTM and DSM, the Canopy Height Model (CHM) for September 2019 UAV-RGB image was estimated by subtracting DTM of February from the DSM of September image and its value ranges from -4.8 to 41.8 cm (Figure 4). We used DTM of February 2020 UAV-RGB image (leaf-on) because of the highest accuracy of the DTM were acquired in the leaf-off season than in the leaf-on season. Note that in the leaf-on season, UAV cannot penetrate the leaves so that few points hit the ground which lead to produce less accurate DTM. In contrast, in the leaf-off season, more points hit the ground as the broadleaved tree species, the dominant tree in the study area, drops their leaves in this season.
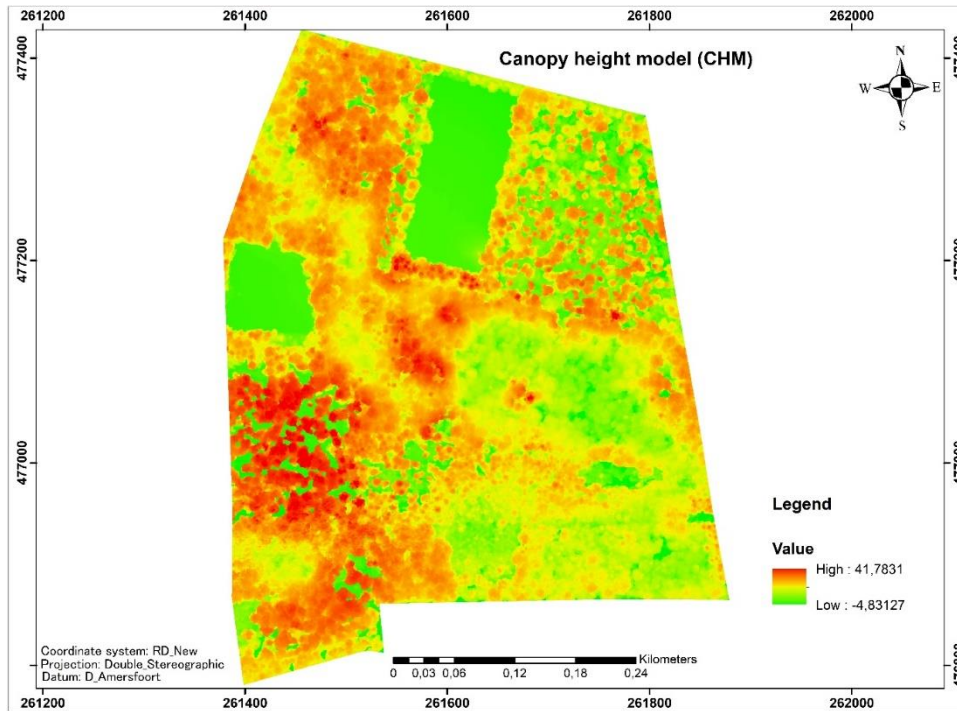
Figure 4: Canopy Height Model (CHM) map

3.3.5. Object-Based Image Analysis

Compared to pixel-based approach, Object-Based Image Analysis (OBIA) showed the highest accuracy result in classifying tree species from the very high spatial resolution remotely sensed imageries (Wang et al., 2018; Kamal & Phinn, 2011). Because of this, OBIA was selected and applied in this study. OBIA was performed in three steps, namely image segmentation, feature extraction, and image classification.

3.3.5.1. Image segmentation

Image segmentation is the first step in OBIA with the aim of segmenting an image into homogeneous objects. In this study, the Multi-Resolution Segmentation (MRS), one of the most widely used segmentation methods in the literature (see section 2.1), was employed in eCogntion developer software. Because of the difficulty in applying the same segmentation parameters for objects of very different sizes, the study area was stratified into two strata: mature and young forest stands. Different rulesets were applied in the two forest stands.

To assess the tree crown segmentation accuracy of the two strata, the UAV imagery captured in September 2019 (leaf-on) was used. This is because the trees have a leaf-on in this season which makes the crown clearly visible. In this study, MRS were applied to segment the tree crowns of the two forest stands by using a combination of CHM and Orthophoto, and Orthophoto only. We have included CHM as a segmentation parameter because CHM can affect the delineation of individual tree crown as tree species exhibit different height (Jakubowski et al., 2013).

The UAV-RGB image captured in September 2019 (leaf-on) was segmented iteratively with the following set (54 combinations) of segmentation parameters: scale (50, 75, 100, 125, 150 and 175), shape (0.4, 0.6, and 0.8) and compactness (0.4, 0.6, and 0.8). In addition to these parameters, CHM layer weight (1, 2, and 3) were also applied so as to assess the effect of combining CHM and Orthophoto (UAV-RGB) on tree crown segmentation. To fix the aforementioned initial scale parameter, the Estimation of Scale Parameter (ESP) tool were used. The ESP tool is integrated with MRS in eCogniation software and segments image object by increasing scale parameters step wisely. ESP tool has user-defined step size parameter, which enables us to increase the segmentation parameters step wisely (Drăguţ et al., 2014). It also calculates the local variance by segmenting each image object in to three levels of homogeneity (from courser to finer). As the scale parameter is not directly associated with certain object size, a trial and error method were employed get the final appropriate scale parameters (Dra, 2010). The graphical user interface of the ESP2 tool which consists of all the parameters is presented in Figure 5. The local variance graph obtained from ESP tool is illustrated in Figure 6. In this study, we used the scale parameter value (red circle in Fig 6) as the initial scale parameter.
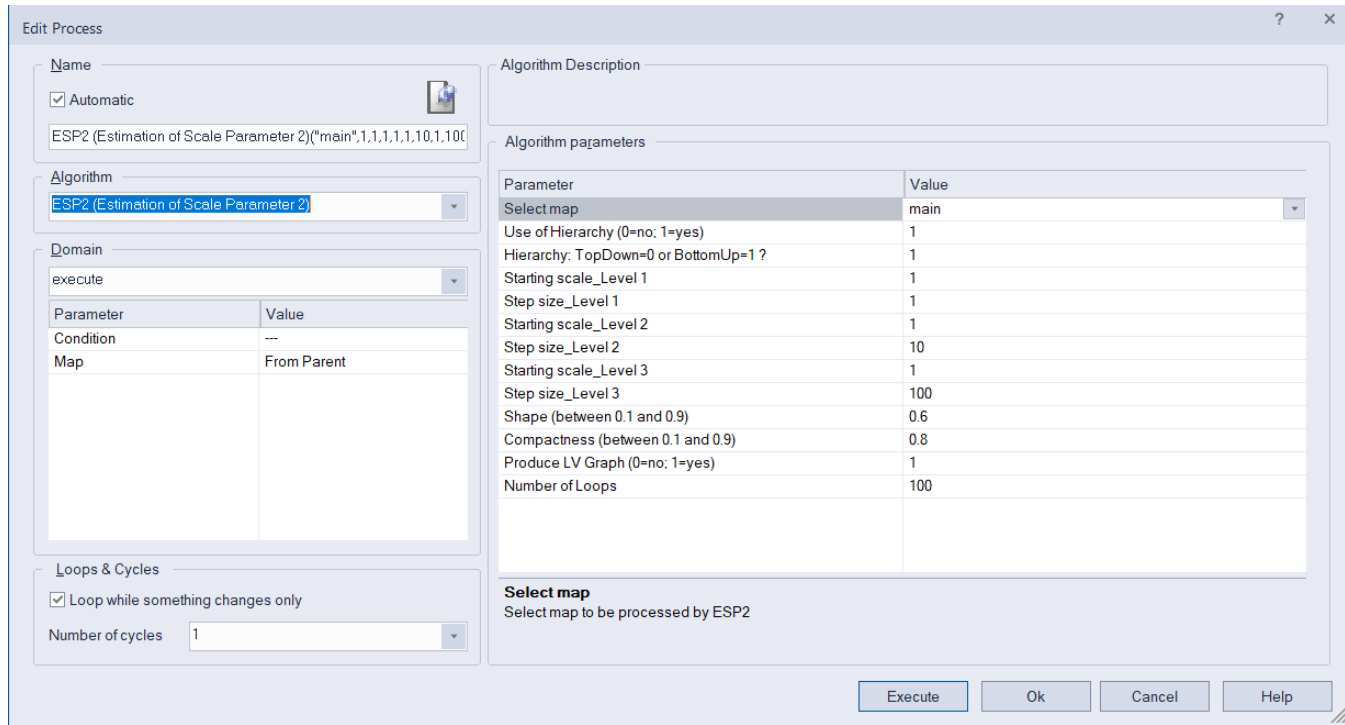
Figure 5: The graphical user interface of ESP2 tool in eCognition software.

Based on the leaf-on season UAV-RGB image, the best segmentation parameter combinations for each forest stand were selected using trial and error. For this, the automatically delineated polygons by MRS were compared against the manually digitized reference tree crown using different segmentation evaluation metrics such as over segmentation, under segmentation and total detection error metrics (for details see section 3.5.1). The combined effect of CHM and Orthophoto on tree crown segmentation were evaluated based on the aforementioned metrics. After this, the best set of segmentation parameters obtained from leaf-on season UAV-RGB image were applied for February 2020 (leaf-off), and a combination of leaf-on

and leaf-off UAV-RGB images. The propagation of the segmentation errors in to the tree species classification may be reduced.
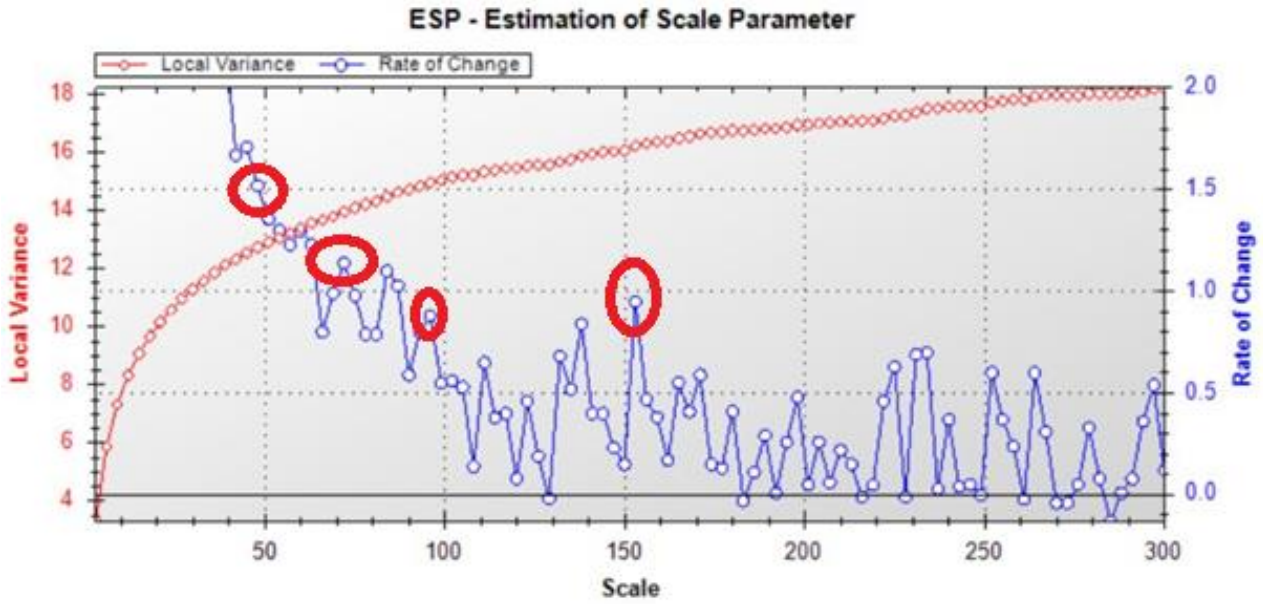
Figure 6: Initial scale parameters estimated by ESP.

3.3.5.2. Shadow Masking and Watershed Transformation

Once the image objects have been created, shadows were separated from trees using the mean brightness value of the segments (96 in our case). Merging algorithms were applied to mask the shadow. After this, the watershed transformation algorithm was employed to solve the under segmentation problems. This under segmentation problem most often occurred when there is an overlapping of tree crowns as it was evident in our study area, particularly in the broadleaved tree species.

In the watershed transformation, the UAV-RGB image is considered as a topographic surface. This algorithm basically applies the basic principle of watershed hydrology, which comprises of three basic notions such as local maxima (tree tops), catchment basins and watershed lines (Chen et al., 2012). The distance of each pixel to the image object border is calculated so as to develop the inverse distance map. Based on the developed map, a pixel which is very far from the image border is identified and considered as the local maxima. Subsequently, the under segmented objects were divided into smaller units based on the given distance of the local maxima or tree top as it is fixed by the size of the largest tree crown. In this study, it was found that the maximum size of trees crown were approximately 7 m, which is 152 pixels in the UAV-RGB image. By giving this threshold value (152 pixels), the cluster of trees (the under segmented tree crowns) were separated, and their individual tree crown were delineated.
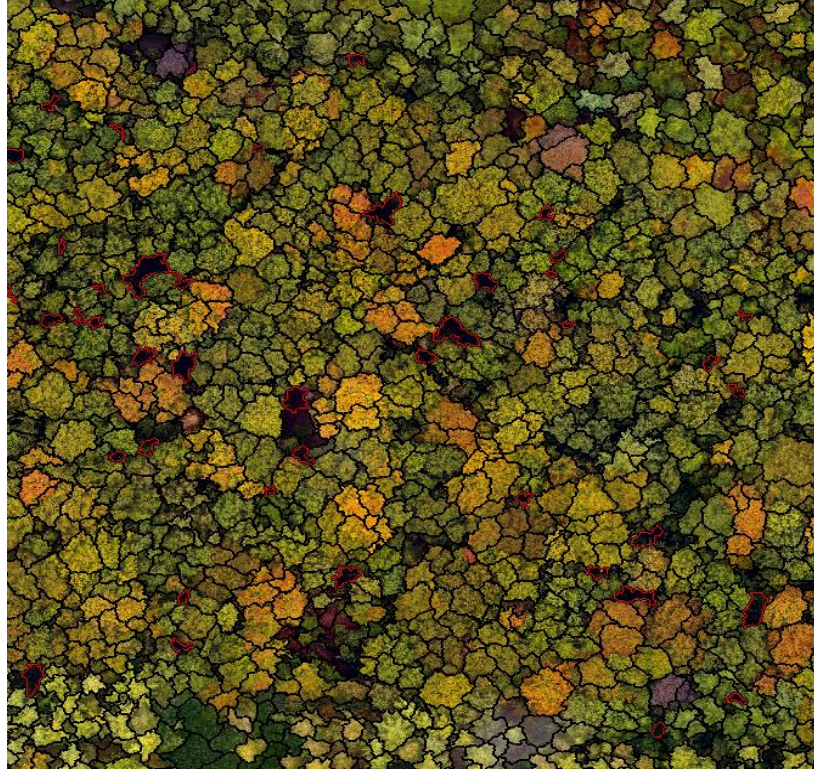
Figure 7: Masking shadow from the tree. The red circles are shadow

3.3.5.3.   Feature extraction

Prior to classifying the tree species using machine learning algorithms, it is very important to extract variables (features) of image objects which are used to separate classes. In this study, a combination of spectral, texture, and CHM variables were selected because multiple features have substantially improved the classification accuracy result as reported in previous studies (Cao et al., 2018; Xie et al., 2019; Zhang et al., 2018). The list of extracted features used for tree species classification under the leaf-on (September 2019), leaf-off (February 2020), and a combination of seasons are presented in Table 5.

Table 5: Selected features for tree species classification.

Seasons	Features/variables
Leaf-on (September 2019)	Mean Red_s, Mean $Green_s$, Mean $Blue_s$, Std. Red_s, Std. $Green_s$, Std. $Blue_s$, Mean CHM_s, $Std.CHM_s$, T-hom-Red_s, T-hom-$Green_s$, T-con-Red_s, T-con-$Green_s$, T-ent-Red_s, T-ent-$Green_s$, T-cor_s –Red_s, and T-cor-$Green_s$
Leaf-off (February 2020)	Mean Red_f, Mean $Green_f$, Mean $Blue_f$, Std. Red_f, Std. $Green_f$, Std. $Blue_f$, Mean CHM_f, Std. CHM_f, T-hom-Red_f, T-hom-$Green_f$, T-con-Red_f, T-con-$Green_f$, T-ent-Red_f, T-ent-$Green_f$, T-cor–Red_f, and T-cor-$Green_f$
A combination of seasons (Sep+Feb)	All the aforementioned variables

Where: s stands for September; f stands for February; std for standard deviation; T for texture; Hom for Homogeneity, con for contrast, ent for entropy; and cor stands for correlation.

In addition to the spectral and CHM variables, the texture of the image object was extracted. The textural features extracted from the segmented object are homogeneity, entropy, correlation and contrast. These statistical features were extracted from the UAV-RGB images using the Gray-Level Co-occurrence Matrix (GLCM) as proposed by (Haralick et al., 1973). GLCM is a statistical approach used to characterize the texture of an image by calculating the spatial relationship of pixels. Accordingly, the homogeneity measures the closeness of the distribution of elements in the GLCM to the GLCM diagonal. Meaning, pixels belonging to one class will have high homogeneity value. The contrast measures the differences in the GLCM which provides information about the heterogeneity of the classes. Similarly, the correlation reflects the joint probability occurrence of the specified pixel pairs, whereas entropy measures the degree of disorder or non-uniformity present in the GLCM. In this study, the texture was extracted from the segmented polygon instead of applying a fixed window such as 3X3 or 5X5, which is commonly applied in pixel-based image analysis. Applying a fixed window size in OBIA may degrade the effectiveness of texture in separating the classes as the texture is highly influenced by the patch size of the given land cover types (Lu et al., 2014).

After image segmentation, all the object features were exported and used for the classification. To do this, a rule set was developed in eCognition under the new processing tree. Export image algorithm was used to extract and export each feature as a separate tiff file since exporting many object features in a batch mode is impossible in eCognition software. About 20 object features from both the leaf-on and leaf-off seasons and 40 object features from the combination of leaf-on and leaf-off season (Table5) were extracted and exported. The object feature values were rescaled to change the values of the features into a common scale so that the effects of higher range feature values on the classification can be reduced (Hsu et al., 2010). In addition to this, the machine learning classifiers perform faster when the data is scaled/normalized. Scaling is a prerequisite in this study as some of the raw data of the extracted features values (e.g. correlation and entropy texture) have lower range values as compared to the spectral and CHM feature values. This analysis was implemented in the R statistical package.

Figure 8 shows the spatial distribution of extracted features from the leaf-on (September 2019) season UAV-RGB image, which were rescaled using equation 1. As indicated in Figure 8, the rescaled mean green feature values range from -3 to 3 in which the grassland shows the higher value (greenish colour) than the other land cover classes. Moreover, this value was different among the tree species to be classified. This indicates that the mean green will partly contribute its parts to separate the class. Similarly, we found that all the image objects have different feature values so that these features contribute their parts in classifying tree species by applying the machine learning algorithms. See Annex 2 and 3 for extracted features for February 2020 and a combination of two UAV-RGB images as well.

$$X = \frac{(Xi - \mu)}{\sigma} - eq1$$

Where X is the scaled image object; Xi is the actual image object values for each feature; μ is the mean value of each feature, σ is the standard deviation value of each feature.
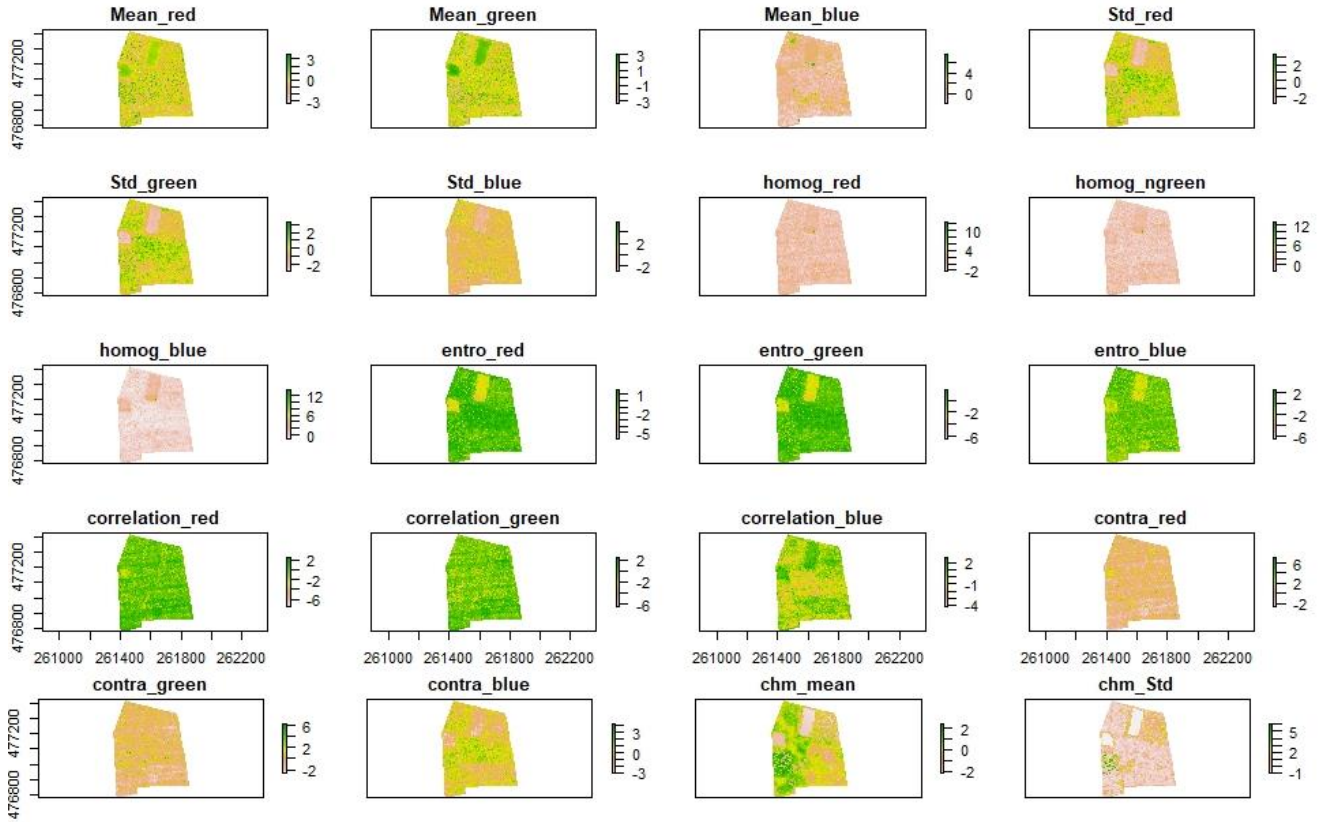
Figure 8: Spatial distribution of features values of image objects extracted from September 2019 UAV-RGB image.

3.3.5.4. Image Classification

Once the image object features are extracted from UAV imageries for different seasons, the next step is classifying tree species using different machine learning algorithms. In this study, three different machine learning algorithms were applied to classify seven tree species, three from the broadleaved and four from the coniferous species. These machine learning algorithms include Support Vector Machine (SVM), Random Forest (RF) and K-Nearest Neighbours (KNN) classifiers. These algorithms were selected because of their effectiveness in producing high classification accuracy result in a mixed forest compared to other machine learning algorithms (e.g. Xie et al., 2019).

Using the UAV-RGB image captured in September 2019 (leaf-on season), all the machine learning algorithms were applied to classify tree species found in a mature mixed broad leave and coniferous forest stand, and their sensitivity for different training sample size was also analysed. Based on the tree classification accuracy assessment metrics (section 3.5.2), comparisons of these classifiers were then made

to identify the best classifiers. Subsequently, the best classifier was applied for February 2020 UAV images (leaf-off season) and a combination of leaf-on and leaf-off season UAV-RGB images so as to analyse the seasonal effect on tree species classification. Note that all the extracted feature variables were used as input for all the machine learning algorithms to classify tree species. In this study, we used a combination of spectral, texture, and CHM features because a single feature cannot separate all the eight classes very well. For example, by using the spectral UAV-RGB image alone, it is very difficult the separate the coniferous tree species that shows similar spectral signatures in the leaf-on season (for details, see section 5.2).

All three machine learning algorithms required the ground truth data to train and test the classifiers. For this purpose, k-fold cross-validation, a statistical method used to estimate the classification skills of machine learning model, were used to reduce human induced bias that may often arise while categorizing the samples in to subsamples (training and testing). In k-fold cross validation, the ground truth data were randomly partitioned into k equal size subsamples. The first k fold is applied to test the classifier, and the remaining k-1 folds are used for the training. In this study, 5-fold cross validation was chosen based on the sample size of the training and test data (247 in our case) we have. In addition, this cross validation has been widely applied in the field of machine learning algorithms. Out of the 5 folds, the 4 folds are used to train the classifier, and the remaining 1 fold is used for testing. In our case, the collected 247 samples were grouped into five equal subsamples of which each subsample comprises around 49 samples. The distribution of each class in the partitioned training and test data were also checked prior to run the classifiers in R statistical package.

A) Support vector machine (SVM)

SVM is a supervised machine learning algorithms which can be used for image classification (Cao et al., 2018; Xie et al., 2019). This algorithm works to separate a number of classes (n-classes) by finding the optimal hyperplane boundary in high dimensional space (Figure 9). SVM use support vectors, data points selected from the training set, that lie closest to the hyperplane boundary. These vectors would help us to build the model and to separate the classes by applying different kernels such as linear, radial basis, sigmoidal and polynomial functions. Using different kernels, the non-linear separable challenges are solved by projecting the data into high dimensional feature space (Bruzzone & Persello, 2009). These kernel tricks make the classifier to be more popular and acceptable in remote sensing fields. Among these kernels, the radial kernel basis function (RBF) were used in this study because of its effectiveness and robustness in separating classes in a higher-dimensional space. In addition, in RBF the non-linearity within the classes are separated better than in the other kernel types (Lin et al., 2005). RBF uses two essential parameters, cost of constraint (C) and gamma (g), to maximize the margin between data points and the hyperplane. C is the regularization parameter that controls the errors of misclassification arising from the training data. The minimal C value indicates the model is poorly fitted while the high value of C shows the problems of overfitting. The other parameter in RBF is gamma, which indicates how far the influence of support vectors

on the decision boundary. Meaning, a high value of gamma means support vectors close to the decision boundary, whereas the low values show the support vectors are far away from the decision boundary (Bruzzone & Persello, 2009). This implies that finding optimal values of C and gamma is indispensable to classify tree species using SVM model. In this study, the C and gamma parameter were fine-tuned using grid search algorithm and 5-fold cross validation in R statistical package. We used C parameter ranges from 10^{-2} to 10^2 and gamma parameter ranges from 0.15 to 2. The optimal values of C and gamma value were selected based on the overall accuracy result as estimated from the confusion matrix (see the attached code in Annex 4 for details).
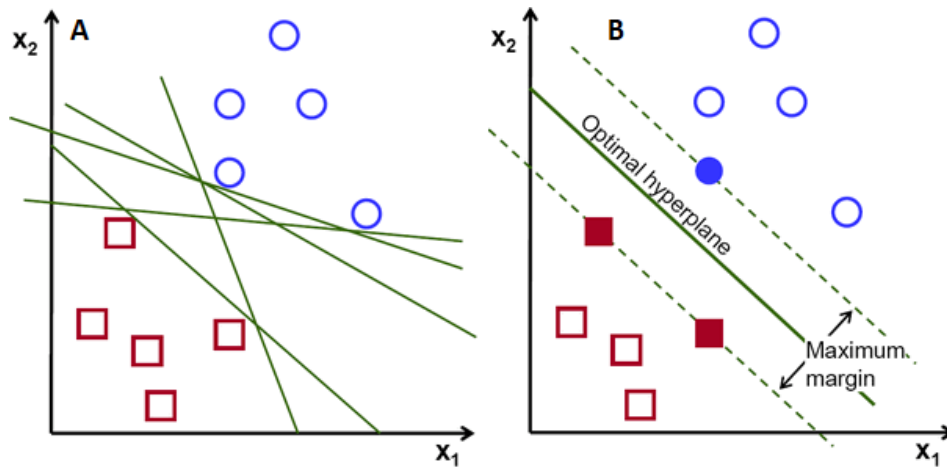
Figure 9: Possible hyperplane (A) and Optimal hyperplane (B) to separate two classes in SVM using a linear kernel. Source: (Towards Data Science, n.d.)

B) K-Nearest Neighbours (KNN)

KNN is one of the simplest supervised machine learning classifiers and widely used for high spatial resolution satellite imageries (Cao et al., 2018; Xie et al., 2019). This machine learning algorithm assigns classes by examining the distance between the K neighbouring samples and unknown object in the feature space (Figure10). If the unknown object is very close to the K neighbouring sample of the known class, this object belongs to the same class. The basic idea behind the classification is that "if you tell me who your neighbours are, I will tell about you". The accuracy of the KNN classifiers mainly depends on the K parameter value. Assigning a small value of K results in higher noise where as a larger value makes the KNN model computationally expensive. Therefore, finding optimal K value is of great importance to acquire best classification result. In this study, optimal K value was automatically determined based on the classification accuracy result as obtained from the different set of K values. The K value, which yields the highest accuracy result, was selected as an optimal K value and then used in object-based KNN classification. The code used in this study is presented in Annex 5.
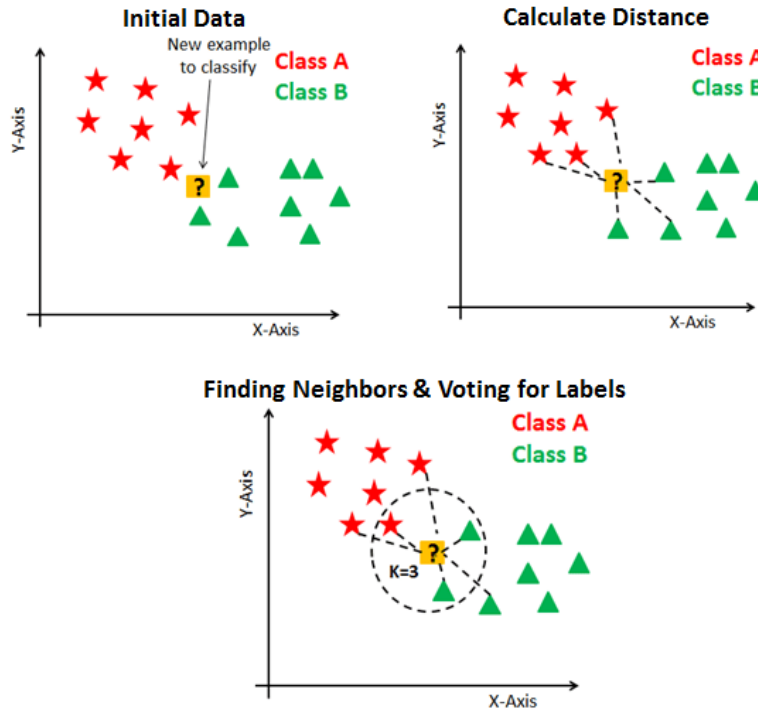
Figure 10: Classification procedure in KNN. Source: (GitHub - artifabrian/dynamic-knn-gpu: Dynamic k-Nearest Neighbours using TensorFlow with GPU support!, n.d.)

C) Random forest (RF)

The RF was developed by Leo Breiman and Adele Cutler, which is mainly used for classification and regression (Breiman, 2001). Its application for natural resource management, including tree species classification, is enormous (Cao et al., 2018; Xie et al., 2019). The workflow of random forest-based classification is presented in Figure 11. Random forest classifier is an ensemble classifier that comprises a large number of individual decision trees. The prediction of each individual each tree were averaged to determine the final prediction of random forest (Belgiu & Drăgu, 2016). As can be shown in Figure 11, each individual tree predicts a class, and the class with the most votes were chosen as a random forest model prediction. The advantage of this classifier is that its robustness to handle many feature /input/ without deletion, its capability to provide variable importance and high classification accuracy result, and its capability to control overfitting.

In random forests, a bootstrap sample from the training set was created randomly to construct an uncorrelated individual tree. About two-thirds of the samples, the bootstrap sample, are used to construct Nth tree. The remaining samples (one-third) are considered as out-of-bag (OOB) samples. This OOB data is used to estimate the unbiased classification error and variable importance. The two important variables of the random forest are ntree and mtry. The ntree indicates the number of uncorrelated trees to grow, whereas the mtry shows the number of variables randomly sampled as candidates at each split. The mtry is the square root of the number of features used to split the node. In this study, the optimal value of the ntree was obtained by fined tuning the model iteratively. The optimal Nth tree gave the lowest OOB error.

Based on the 20 features extracted from the leaf-on and leaf-season and 40 features from the combination of leaf-on and leaf-off seasons, the corresponding mtry value for those seasons is equal to 4 and 6. Moreover, the variable importance, one of the important components of the random forest classifiers, were determined using the mean decrease in Gini (MDG) and mean decrease accuracy (MDA) metrics. MDG estimates how much a variable reduces the Gini impurity metric in a particular class (Lim et al., 2019). The Gini impurity of a node shows the numbers of incorrectly labelled samples (features) in a node from a randomly selected sample in the corresponding node. The MDA considers the difference OOB error which is resulted from the original dataset and from random variation of the value of different variable. Based on the variable importance results, the most important variables or features were selected by observing the MDG results. This result enable us to get best tree species classification result. For details, kindly see the script in annex 6.
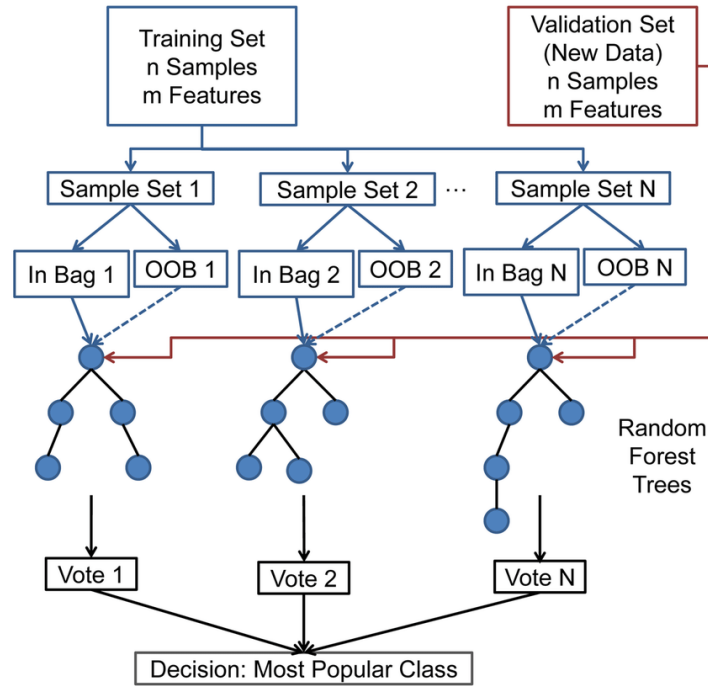
Figure 11: Classification procedure in a random forest (adapted from Liarokapis et al., 2013). OOB stands for out-of-bag.

3.4. Data analysis

3.4.1. Segmentation accuracy assessment

Following Clinton et al., (2010), the area estimation technique was used to assess the segmentation accuracy of tree crowns delineated from a combination of CHM and Orthophoto, and Orthophoto only. The over segmentation, under segmentation and total detection error (segmentation error), were quantified for both mature and young forest stands (Eq1-3). The ideal value of the over segmentation, under segmentation and

total detection error is 0. The reference polygons (tree crowns) were manually digested in ArcGIS for two forest stands and then applied to quantify the segmentation error.

$$over\ segemation(X) = 1 - \left(\frac{area(ASI\ \cap AMP)}{area(ASI)}\right) - - - - - - - - - - - - - - - - - eq1$$

$$under\ segemation(Y) = 1 - (((area(ASI\ \cap AMP))/area(AMP)\ ) - - - - - - - - - -eq2$$

$$Total\ detection\ Error(segementation\ error) = \sqrt{\frac{(X^2 + Y^2)}{2}} - - - - - - - - - - - -eq3$$

Where;

ASI is an area of the segmented object by multi-resolution segmentation algorithms (MRS)

AMP: area of the reference polygon (tree crown) which is manually digitized in ArcGIS

Area (ASI ∩AMP): area of manually delineated polygon correctly identified by MRS

3.4.2. Classification Accuracy Assessment

The accuracy of SVM, RF and KNN classifiers in classifying seven tree species and one non-tree class were examined using the confusion matrix. The overall, the producer, and the user accuracy were quantified from confusion matrix that were developed fron the K-fold validation. For this, we used 5-fold cross validation that produces one confusion matrix for each fold. The tree species classification accuracy assessment were employed based on the final confusion matrix by adding all the five confusion matrix.

4. RESULTS

4.1.   Tree Crown Delineation by Combining September 2019 Orthophoto and CHM

In this section, results related to tree crown segmentation using Multi-resolution segmentation algorithm, including a selection of the best combination of segmentation parameters, and segmentation accuracy assessment in the two forest stands are presented.

4.1.1. Selection of the best segmentation parameter combinations

After a thorough trial and error, the best segmentation parameter combinations in delineating tree crowns of mature and young forest stands were identified, and results are presented in Table 6. Using the September Orthophoto only, the best scale, shape and compactness parameters for mature (young) forest stands were 150 (50), 0.6 (0.6) and 0.8 (0.6), respectively. The same scale and compactness parameter values were identified in delineating the tree crowns of the two forest stands when combining Orthophoto and CHM. In addition to this, the tree crown segmentation were also performed by changing the weight given to the CHM layer. We found the best segmentation result when the CHM layer weigh was given as 1. As indicated in Figure 12 and 13, based on our visual inspection, the tree crown segmentation accuracy worsened as the CHM layer weight increased from 1 to 3 in both forest stands. As a result, over segmentation prevails in both forest stands (Figure 12 and 13).

Table 6: Best segmentation parameter combinations in delineating tree crowns of the two forest stands.

Forest stand	Species group	Orthophoto only			Combinations of Orthophoto and CHM			
		Scale	Shape	Compactness	Scale	Shape	Compactness	CHM weight
Mature	Broadleaved	150	0.6	0.8	150	0.4	0.8	
	Coniferous	150	0.6	0.8	150	0.4	0.8	1(optimal weight)
Young	Broadleaved	50	0.6	0.6	50	0.4	0.6	
	Coniferous	50	0.6	0.6	50	0.4	0.6	

Since scale is the most sensitive parameter that considerably affects the segmentation accuracy result (Drăguţ et al., 2014; Zhang et al., 2008), we evaluated the effect of scale on tree crown segmentation by changing shape, compactness and CHM weight parameters for the given scale. Figure 14 shows results of the over segmentation, under segmentation and total detection error (segmentation error) of the tree crown segmentation in a changing scale parameters. This analysis was performed in the mature forest stand as this forest stand produced the highest segmentation accuracy result (Table7). The boxplot results showed that the tendency of over segmentation decreases as the scale parameter increase from 50 to 150, but it shows an increasing trend as the scale parameter increases from 150 to 175. In contrast, the under segmentation increase as the scale parameter increase from 50 to 100 and then reached maximum when the scale parameter is 100. The lowest total detection error was recorded when the scale parameter were given 125, 150 and

175, and their corresponding median value is 0.22, 0.186, and 0.218, respectively. Similarly, the lowest over segmentation result was produced when the scale parameter is about 125, 150 and 175 with a median value of 0.19, 0.17 and 0.21, respectively. In contrast to this scale, the lowest under segmentation errors were reported when we applied the scale parameter of 50, and 75 with a median value of 0.14 and 0.18, respectively.
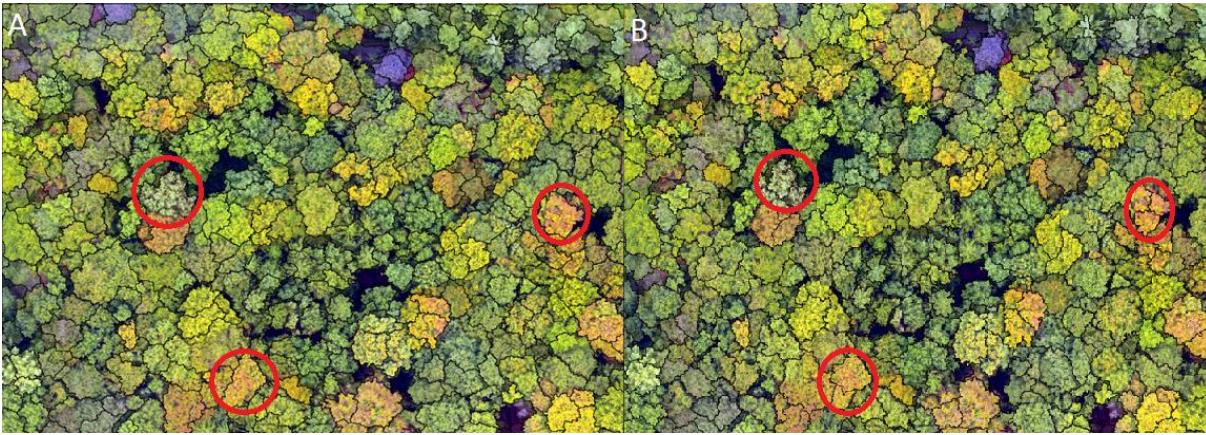
Figure 12: Tree crown segmentation using a combination of Orthophoto (leaf-on) image and CHM. The weight of CHM layer were given to 2 (A) and 3 (B) in the mature forest stand. The red circle shows the observed difference in segmentation in varying CHM layer weight based on our visual inspection assessment.
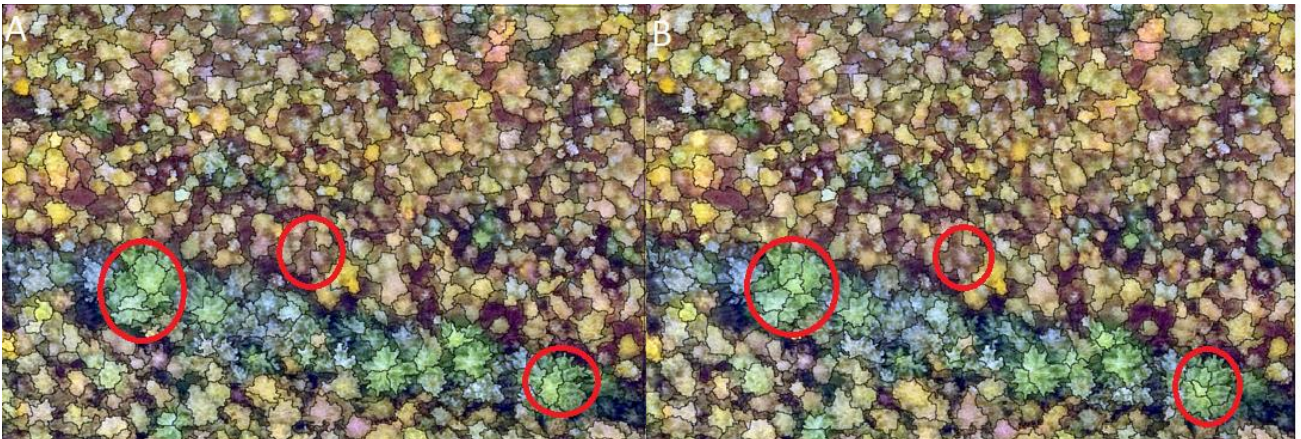
Figure 13: Tree crown segmentation using a combination of Orthophoto and CHM in a changing CHM layer weight from 2 (A) to 3 (B) in young forest stand. The red circle shows the observed difference in segmentation based on our visual inspection assessment.
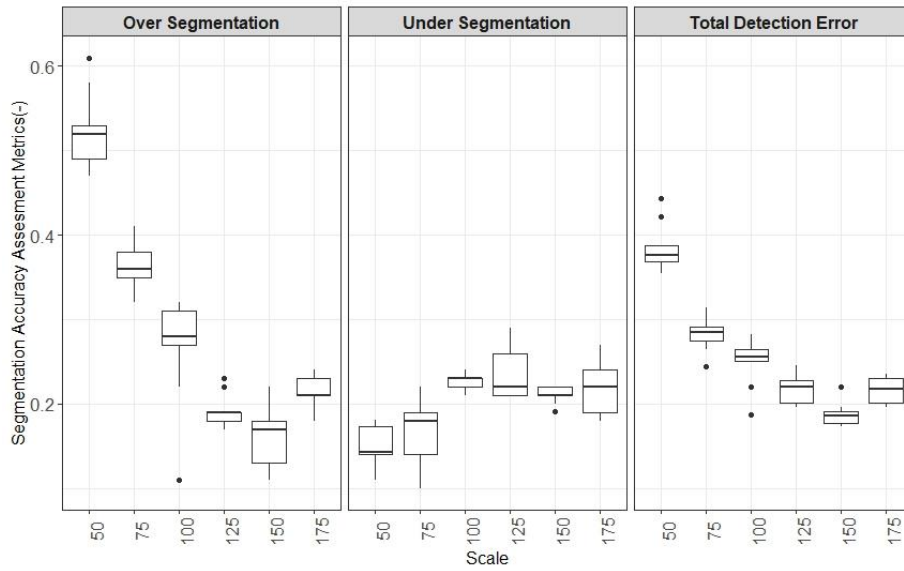
Figure 14: Segmentation accuracy in the mature forest stand in a changing scale parameter using the leaf-on season (September 2019) UAV-RGB image. The horizontal line of the box plot shows the median values, whereas the top and bottom lines indicate 25th and 75th percentile. The black dots show the outlier.

4.1.2. Segmentation accuracy assessment

The tree crown segmentation accuracy of the two forest stands using a combination of Orthophoto and CHM, and a single Orthophoto is presented in Table 7 and Figure 15. Results revealed that combining Orthophoto and CHM improved the tree crown segmentation of the young mixed forest stand by 3% whereas their performance were reduced by 1% in the mature forest stand. Specific to the broadleaved and coniferous tree species of the two forest stands, the combination of CHM and Orthophoto improved the tree crown segmentation of coniferous species by 1% and by 9% in mature and young forest stands, respectively. However, they did not improve the tree crown segmentation of the broadleaved species, the dominant tree in the study area. This is mainly associated with the accuracy of the UAV derived CHM, which is lower in a mature mixed forest stand than in the young forest stand. The low accuracy of CHM in the mature forest stand may be attributed to the accuracy of digital terrain model.

On average, both Orthophoto and a combination of CHM and Orthophoto produced the highest tree crown segmentation result in a mature forest stand than in young forest stand. In mature broadleaved and coniferous forest stand, tree crowns were better delineated by single Orthophoto (83%) than by a combination of CHM and Orthophoto (82%) (Figure15). In contrast, the tree crown delineation of the young forest stand was improved when we are combining CHM and Orthophoto instead of applying Orthophoto only. In general, the lowest segmentation accuracy were reported from the young mixed forest stand. This is mainly attributed to the existence of the randomly distributed mature deciduous and coniferous species in the young forest stand, which in turn affect the optimized scale parameters assigned

for this forest stand. Based on the aforementioned findings, we reject the null hypothesis for the young forest stand as a combination of Orthophoto and CHM improves the tree crown segmentation result in young forest stand by 3%. In contrast, we accept the null hypothesis for mature forest stand as a combination of Orthophoto and CHM doesn't improve the tree crown segmentation.

Table 7: The tree crown segmentation accuracy assessment result based on September 2019 (leaf-on) Orthophoto. The numbers in bracket indicate the segmentation accuracy result obtained by combining CHM and Orthophoto.

Forest stand	Species group	Segmentation Accuracy Assessment Metrics			
		Over segmentation	Under Segmentation	Total Detection Error	Accuracy (%)
Mature	Broadleaved	0.12 (0.14)	0.23 (0.26)	0.18 (0.21)	82 (79)
	Coniferous	0.13 (0.16)	0.22 (0.12)	0.18 (0.14)	83 (84)
Young	Broadleaved	0.13 (0.08)	0.17 (0.25)	0.15 (0.18)	85 (82)
	Coniferous	0.08 (0.08)	0.55 (0.43)	0.39 (0.3)	61(70)

Combination of Orthophoto and CHM in mature forest stand(Overall accuracy: 82%)	Orthophoto only in mature forest stand (Overall accuracy: 83%)
Combination of Orthophoto and CHM in young Forest stand (Overall accuracy: 76%)	Orthophoto only in young forest stand (Overall Accuracy: 73%)
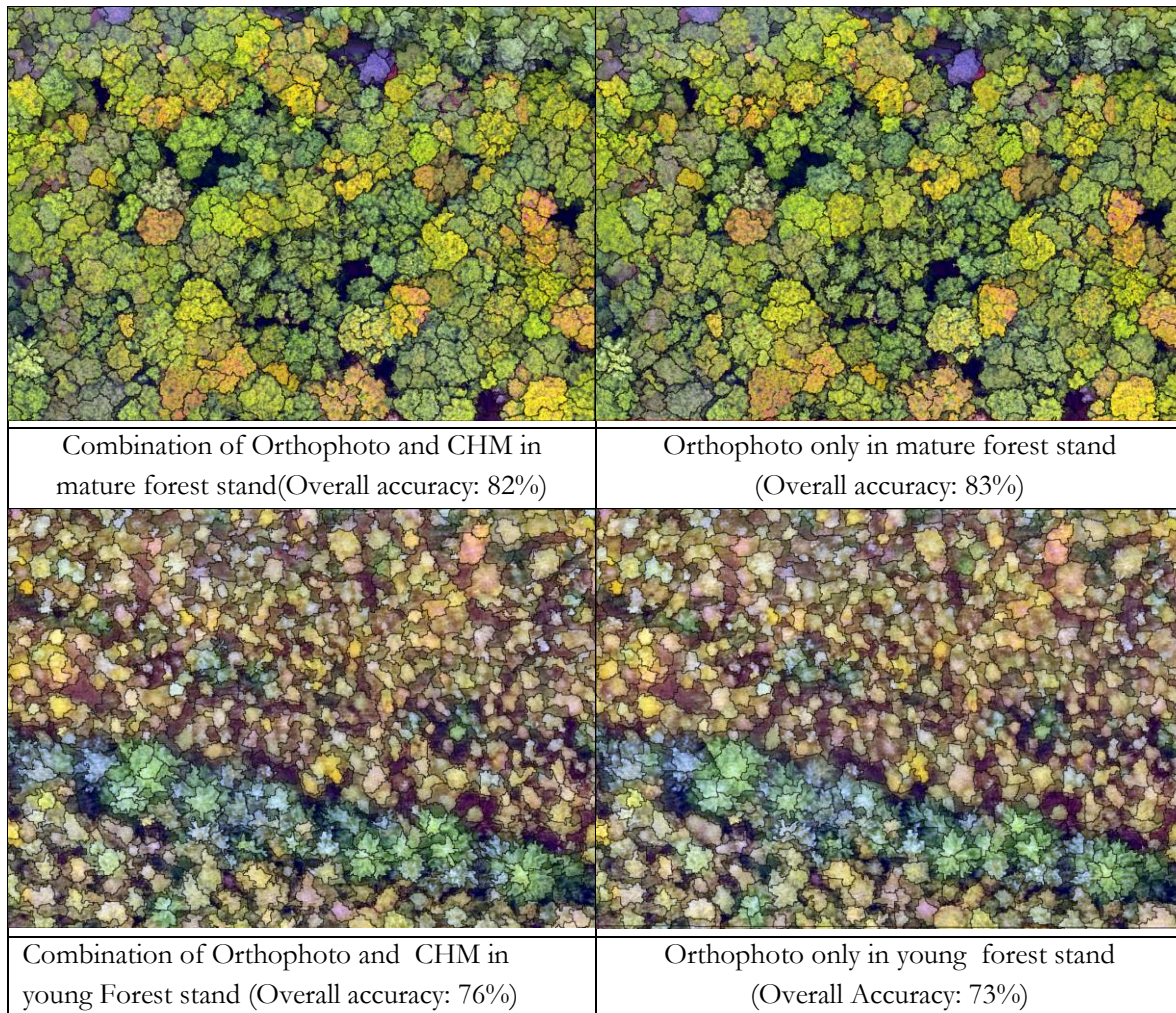
Figure 15: Overall tree crown segmentation accuracies of the two forest stand using a combination of Orthophoto and CHM, and Orthophoto only.

4.2. Comparison of machine learning algorithms in classifying tree species using leaf-on UAV-RGB image, September 2019 image

Table 8 shows results of Random Forest (RF), Support Vector Machine (SVM) and K-nearest neighbour (KNN) object-based classification by using a combination of spectral, texture and CHM object variables. Results show that the SVM outperformed the KNN and the RF classifiers. The SVM object-based classification produced the highest performance with an overall accuracy (OA) and a kappa coefficient of 79% and 0.75, respectively. As compared to KNN and RF, the SVM classifier gave the highest producer accuracy for all tree species except for Larch, which showed the highest producer accuracy result in Random Forest.

Table 8: Summary of tree species classification accuracies using Random Forest, Support vector machine and K-nearest neighbour object-based classification for the leaf-on season UAV-RGB image. The best result obtained from these machine learning algorithms for each tree species and species group are in bold.

Species group	Classified tree species	Random Forest		Support Vector Machine		K-Nearest Neighbour	
		PA%	UA%	PA%	UA%	PA%	UA%
Coniferous	Douglas fir	69.56	78.04	**76.08**	**85.36**	64.15	82.92
	Pine	38	23	**54**	**32**	50.00	23
	Spruce	54.54	33.33	**68.75**	61.11	63.15	**66.66**
	Larch	**80 .00**	55.17	72.72	**55.17**	57.14	41.37
Broadleaved	Oak	68.96	90.90	**73.07**	**86.36**	62.71	84.09
	Beech	95.00	95.00	**100**	**95.00**	96.55	70.00
	Birch	88.23	90.31	**94.11**	**92.17**	82.35	84.21
Non-tree		76.19	55.17	79.06	94.44	84.61	91.66
OA %		OA for both spp.:74.4 OA for conf: 53.63 OA for Broad: **92.07**		OA for Both: **79** OA for conf.: 62.72 OA for Broad: 91.08		OA for both spp.:70.85 OA for conf: **73.38** OA for Broad: 67.46	
Kappa		0.7		0.75		0.66	

Similarly, the SVM classifier has also produced the highest user accuracy (UA) result for all tree species except, Oak which is best classified (best user accuracy) in Random Forest. Compared to the broadleaved tree species, SVM and RF reported low values of overall accuracy in classifying Coniferous tree species, but KNN produced the highest accuracy for this species. The reason for the low performance result of coniferous species in all machine learning algorithms is that the canopies of coniferous species are covered by the dominant broadleaved tree species. Moreover, the performance of all classifiers was poor in discriminating Pine species and gave a producer accuracy (PA) result ranges from 38% to 54% and a user accuracy ranges from 23% to 32%. This is mainly associated with the resembled spectral reflectance of this species with other coniferous species such as Douglas fir, Spruce and Larch (see the discussion part particularly the spectral profile image, Figure 22). In addition, the overall accuracy of each classifier per species group is indicated in Table 8. Results showed that the broadleaved tree species are best discriminated

by random forest algorithms whereas the KNN model shows the highest accuracy for coniferous species group. However, in a mixed coniferous and broadleaved forest stands, SVM produced optimal results to classify all the tree species. Specific to the individual tree species, we found the highest producer and user accuracy for Beech species in all machine learning algorithms except KNN which produced low user accuracy for this species. Similarly, Spruce was best separated in SVM and KNN object-based classification with the highest producer accuracy of 69%, and user accuracy of 67%, respectively. For Larch species, random forest produces the highest producer (80%) and user accuracy (55%) which is similar to SVM classification. Overall a cost effective UAV-RGB image has a capability to discriminate tree species as explained by an overall accuracy of greater than 70%.

Fine tuning of model parameter and variable importance were also performed and results are presented from figures 16-18. The cost and gamma parameters of the SVM classifier was fine-tuned between 0.15 and 2 for gamma, and from 0.01 to 100 for cost in R statistical package. We found the highest tree species classification result when the cost is 10 and gamma is 0.32. The total support vectors produced by SVM are about160 of which 26 for the non-forest area, 23 for beech, 18 for Spruce, 25 for pine, 21 for Douglas Fir, 10 for Oak and 14 for Larch. These support vectors were used by the model for based-object based tree species classification. For RF classifier, the most important variables among the 20 object feature values were selected, and the result are shown in Figure 16. Based on the mean decrease accuracy and Gini index results, the mean red, mean blue, entropy green, entropy red and CHM mean are the most important variables for the RF object-based classification. Moreover, one of the multiple decision trees (500) used by the random forest classifier is also shown in Figure 17. RF use the average prediction of those 500 trees to predict the classes. Similarly, in KNN classifiers, the highest K (neighbour) value was selected based on the overall accuracy as shown in Figure18. The confusion matrix produced by each machine learning algorithm are attached in Annexes 8 to 11. The area coverage of each tree species classfied by SVM classfier using leaf-on season UAV-RGB image is presented in Annex12.
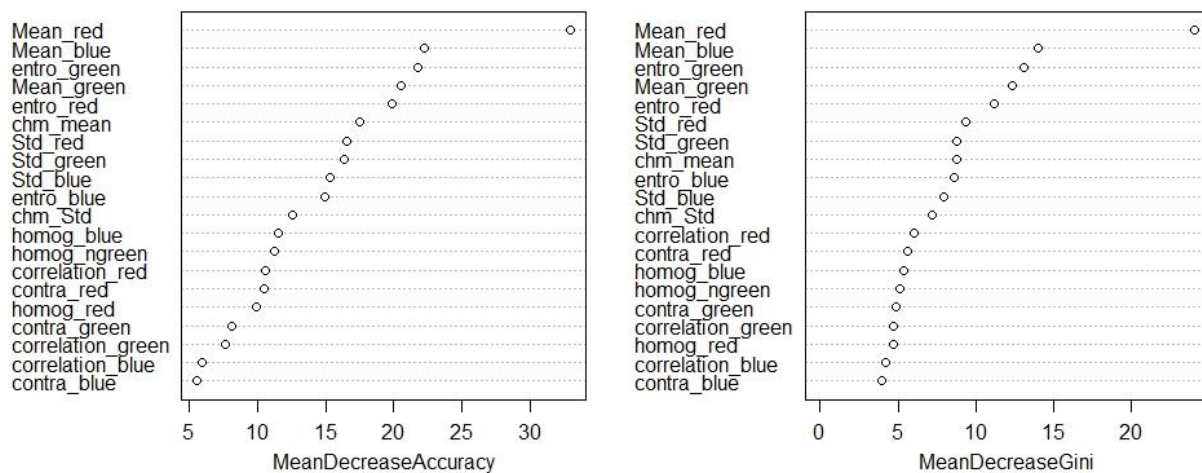
Figure 16: Variable importance result from the random forest classification.
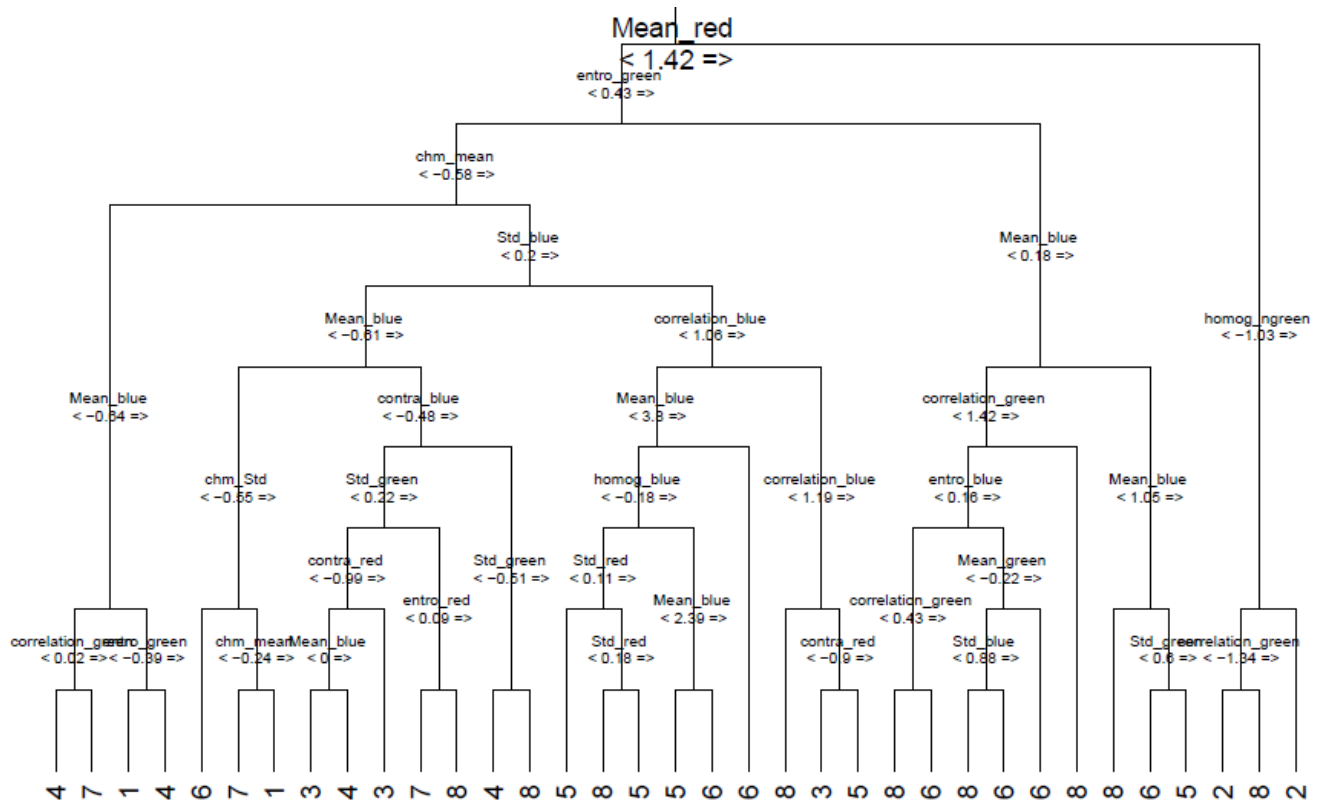
Figure 17: One of the decision trees produced by the random forest. The numbers at the bottom of the tree indicated the classes (non-tree area (1); Beech (2), Larch (3), Pine (4): Douglas fir (5): Oak (6): Birch(7) and Spruce(8)).
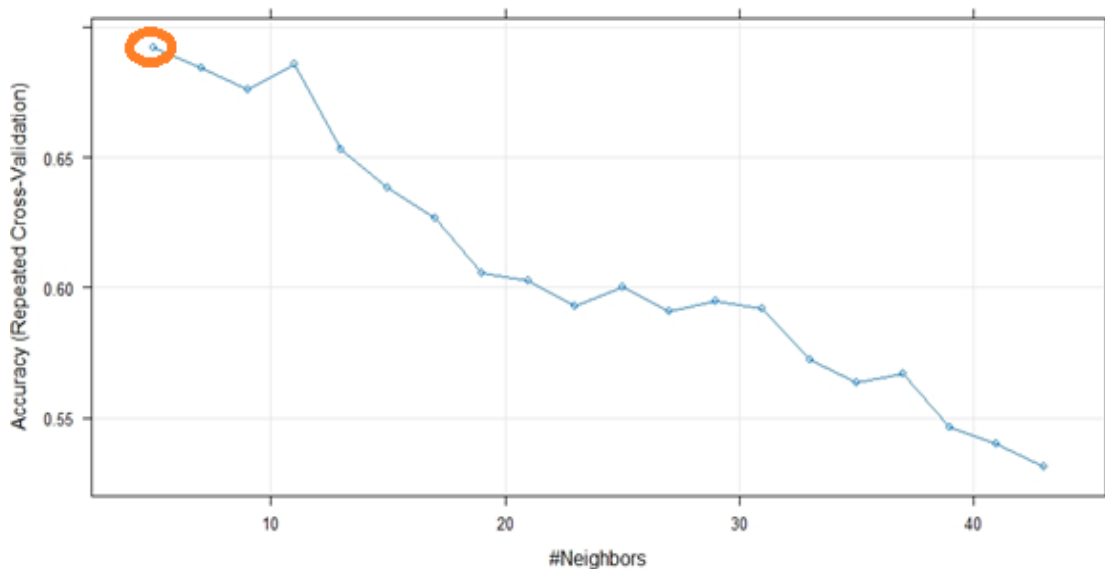
Figure 18: Fine-tuning of K (neighbours) in the KNN classifier. The red circle shows the optimized K value (K=5) used for object-based KNN trees species classification.

Figure 19 shows the spatial distribution of the classification results obtained from the RF, KNN and SVM object-based classification. The performance of all the classifiers in terms of representing the actual

distribution of seven tree species were outstanding. As per our visual inspection, SVM produced better spatial distribution map similar to the original image. In general, the overall accuracy result is sufficient to reject the null hypothesis and accept the alternative hypothesis set in this study "SVM outperforms RF in classifying tree species using the leaf-on season UAV-RGB image."
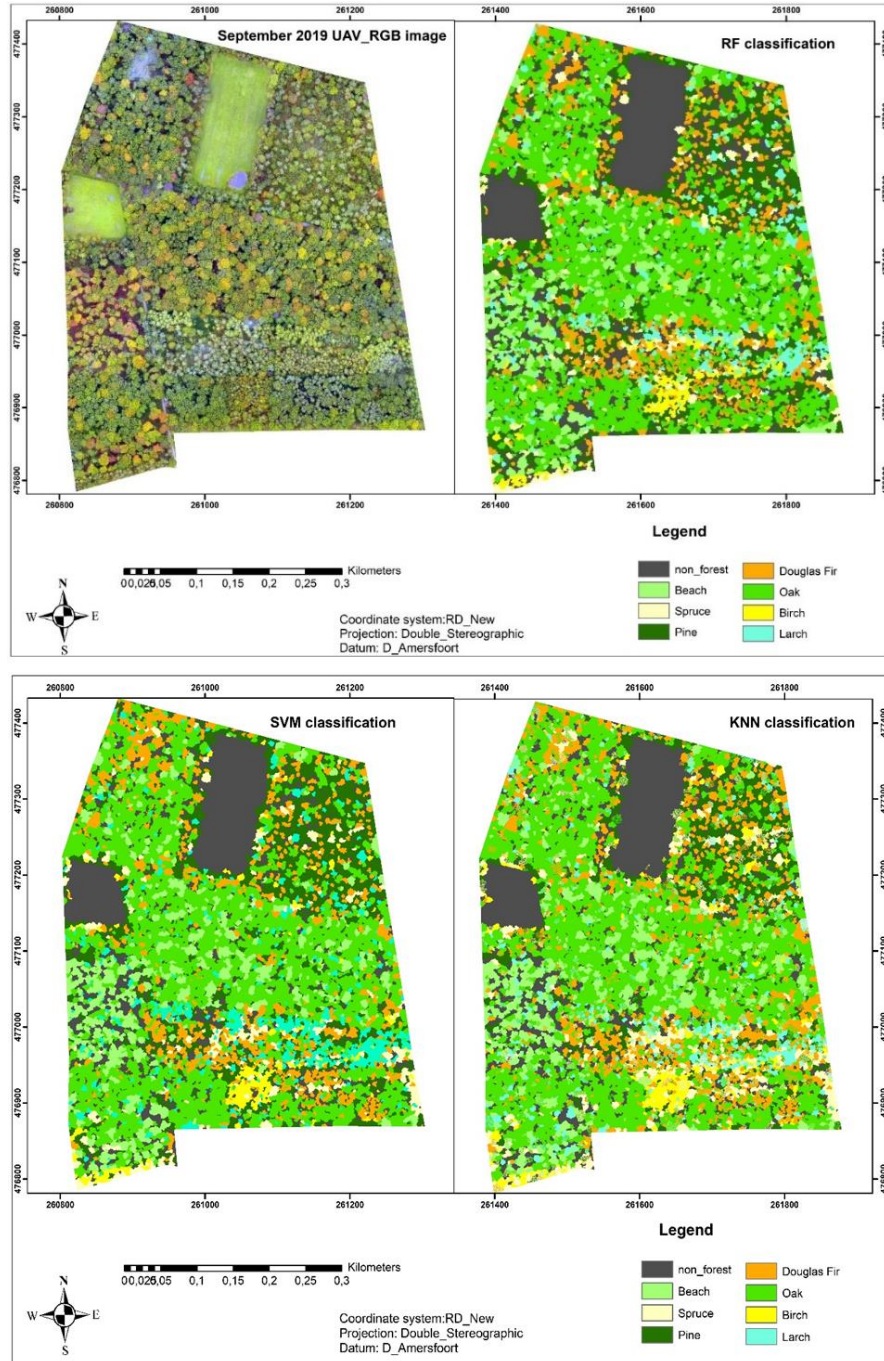
Figure 19: Spatial distribution of tree species classification under the leaf-on condition using RF, KNN, and SVM classifiers.

4.3. Accuracy of tree species classification using UAV-RGB images of Leaf-on and Leaf-off seasons

The result of SVM object-based tree species classification under the leaf-on and leaf-off conditions is presented in Table 9. Note that September 2019 UAV and February 2020 UAV-RGB images represent the leaf-on and leaf-off seasons, respectively. Prior to comparing the seasonal effect on tree species classification accuracy result, the February image was segmented using a different set of parameter combination including the best segmentation parameter combinations obtained from UAV September 2019 image. Based on our visual inspection assessment, fortunately, the best segmentation parameter combinations obtained from September UAV-RGB image (scale=150, shape=0.6 and compactness=0.8) gave an accurate segmentation result for February 2020 UAV-RGB image as well. Subsequently, about 20 object features were extracted from February 2020 to classify tree species using SVM classifier. Results show that SVM object-based classification produced the highest overall accuracy of 65% for coniferous species in the leaf-off season (February 2020 UAV-RGB image). The optimized values of cost and gamma parameters of the model fine-tuned from the February image are 15 and 0.5, respectively. As expected, the leaf-off season improves the classification of coniferous species groups as compared to the leaf-on season.

Table 9: Summary of tree species classification accuracies using SVM for leaf-on and leaf-off seasons. The best performance evaluation result for each tree species and species group are in bold.

Species group	Classified tree species	Leaf-on season (September 2019 image)		Leaf-off season (February2020 image)	
		PA	UA	PA	UA
Coniferous	Douglas fir	76.08	**85.36**	**76.74**	80.48
	Pine	53.84	31.81	**62.50**	**45.45**
	Spruce	**68.75**	**61.11**	66.66	44.44
	Larch	72.72	55.17	**80.0**	**68.96**
Broadleaved	Oak	**73.07**	**86.36**	62.06	81.81
	Beech	**100**	**95.00**	73.17	75.00
	Birch	**94.11**	**92.17**	62.50	58.82
Non-tree		79.06	**94.44**	**80.55**	80.55
OA(%)		OA for both species: **78.94** OA for Coniferous: 62.72 OA for broadleaved:**91.08**		OA for both species: 71.25 OA for Coniferous: **64.54** OA for broadleaved: 75.24	
Overall Kappa		0.70		0.65	

The leaf-off season improved the coniferous tree species classification by 1.82% because of the absence of the dominant broadleaved tree species in this season. Most of the tree species grouped under coniferous types showed the highest producer and user accuracy in the leaf-off season than in the leaf-on season. In contrary, the leaf-off season did not improve the broadleaved species group as compared to the leaf-on season. Specific to the coniferous species, all coniferous species except Spruce are better separated in the leaf-off season than in the leaf-on season. Pine and Larch are best differentiated in the leaf-off season UAV-

RGB image with a producer accuracy of 63%, and 80 %, respectively and a user accuracy of 45% and 69%, respectively. In general, based on the overall accuracy results, the leaf-on season outperformed the leaf-off season in classifying all tree species except the coniferous ones. The coniferous species particularly Pine and Larch are well discriminated in the leaf-off season whereas the broad leaf species are separated better in the leaf-on season than in the leaf-off season.

Figure 20 shows the spatial distribution of the classified tree species under the leaf-on (September image) and leaf-off (February image) conditions. Results revealed that the distribution of broadleaved tree species in the leaf-off season is similar to the leaf-on season. However, the distribution of coniferous tree species in the leaf-on and leaf-off season varied spatially. Based on our visual inspection, the distribution of coniferous tree species were best represented in the leaf-off season than the leaf-on season. Some of the non-forest areas were mixed with broadleaved tree species in the leaf-off season which may be attributed to the similarity of the spectral characteristics of broadleaved tree species and the non-forest area.
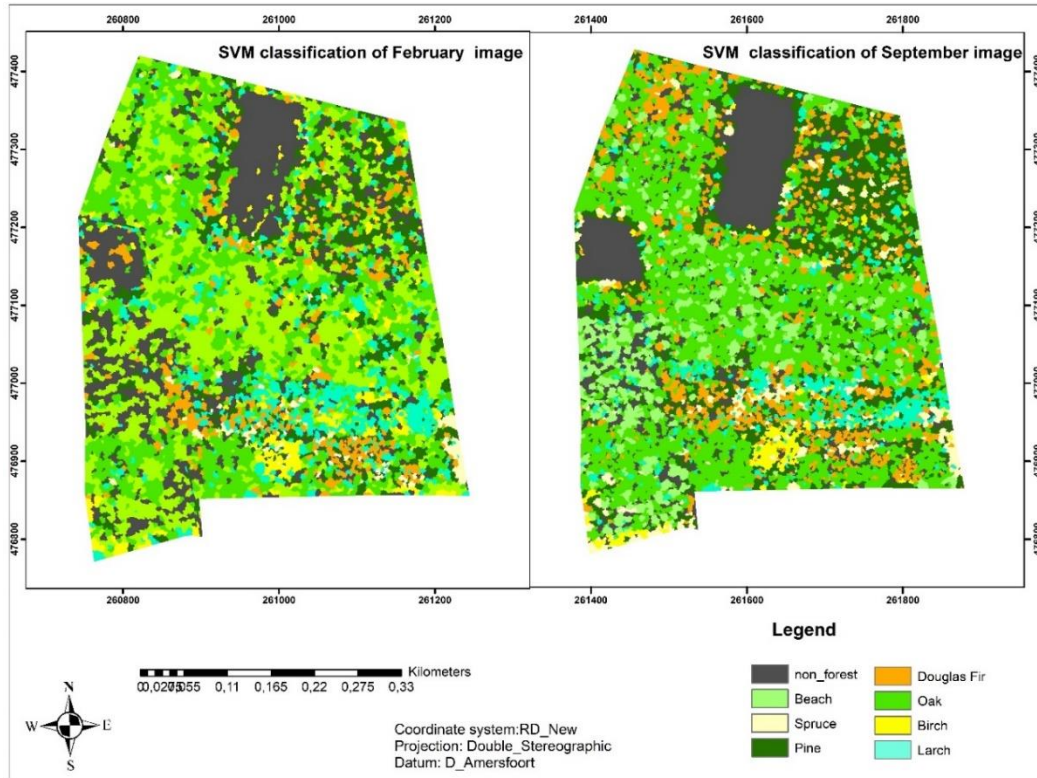
Figure 20: Spatial distribution of tree species classification using SVM classifier for leaf-off (February) and leaf-on (September) image.

4.4.   A combination of Leaf-on and Leaf-off season UAV-RGB images in classifying tree species

The classification result obtained from a combination of two seasonal UAV-RGB images is presented in table 10 and the results are compared with the leaf-on and leaf-off season UAV-RGB image. Based on the overall accuracy result, a combination of two UAV-RGB images, a combination of all bands from a different

season, produced an overall accuracy of 83% and a kappa coefficient of 0.75. This indicates that a combination of two UAV-RGB images improves the classification accuracy result as compared to a single date UAV-RGB image. It improves the leaf-on season (September 2019 UAV-RGB) and the leaf-off season (February 2020 image) tree species classification by 3.7% and by 11.3%, respectively. Most of the coniferous species are better identified in a combination of two UAV-RGB images than a single date image (February 2020 or September 2019). For instance, considering the user accuracy results obtained from the leaf-on season, the separability of Douglas fir were improved from 85% to 93% when a combination of leaf-on and leaf-off season UAV-RGB images used. Similarly, Pine species was improved from 32% (leaf-on) and 45% (leaf-off) to 48%. Similarly, a combination of two UAV-RGB images improved the producer accuracy results obtained from a single date UAV-RGB image. Moreover, Pine tree species cannot be easily identified when a single date UAV-RGB images (leaf-on and leaf-off) or a combination of two UAV-RGB images used. This may be associated with a similar spectral reflectance of this species with the remaining tree species.

Table 10: Comparison of a combination of seasonal UAV-RGB image against the leaf-on and leaf-off season UAV-RGB image in classifying tree species using SVM classifier.

Species group	Classified tree species	Leaf-on season		Leaf-off season		Combination of Seasons	
		PA %	UA%	PA %	UA %	PA%	UA %
Coniferous	Douglas fir	76.08	85.36	76.74	80.48	**81.25**	**92.85**
	Pine	53.84	31.81	**62.50**	45.45	55.14	**47.67**
	Spruce	68.75	61.11	66.66	44.44	**92.30**	**66.66**
	Larch	72.72	55.17	80.0	**68.96**	**80.95**	58.62
Broadleaved	Oak	73.07	86.36	62.06	81.81	**78.72**	**84.09**
	Beech	**100**	**95.00**	73.17	75.00	86.04	92.50
	Birch	**94.11**	**92.17**	62.50	58.82	83.33	88.23
Non-tree		79.06	94.44	80.55	80.55	**88.88**	**88.88**
OA %		OA for both spp.:78.94 OA for Conf: 62.72 OA for broad: **91.08**		OA for both spp: 71.25 OA for Conf: 64.54 OA for broad: 75.24		OA for both:**82.59** OA for conf: **75.45** OA for broad: 88.11	
Kappa		0.70		0.65		0.75	

In general, the combination of two UAV-RGB images improved the overall classification accuracy, and this improvement is more pronounced for coniferous tree species group. Using a combination of leaf-on and leaf-off UAV-RGB image, we found an overall accuracy of 75% for coniferous and 88% for broadleaved species group. Compared to the leaf-on season UAV-RGB image, the combination of two UAV-RGB images did not much improve the broadleaved species.

Figure 21 shows the spatial distribution of all tree species classification in a combination of leaf-on and leaf-off season UAV-RGB images. Results revealed that the spatial distribution of Douglas fir (Orange colour) were considerably varied in September 2019 UAV-RGB image (leaf-on) than in February image (leaf-off) and a combination of two UAV-RGB images. This result is explained by the producer and user accuracy as

indicated in Table 10. According to the overall accuracy and kappa coefficient results, the null hypothesis is rejected in support of the alternative hypothesis that the combinations of leaf-on and leaf-off season UAV-RGB images improve the tree species classification result as compared to a single season UAV-RGB image.
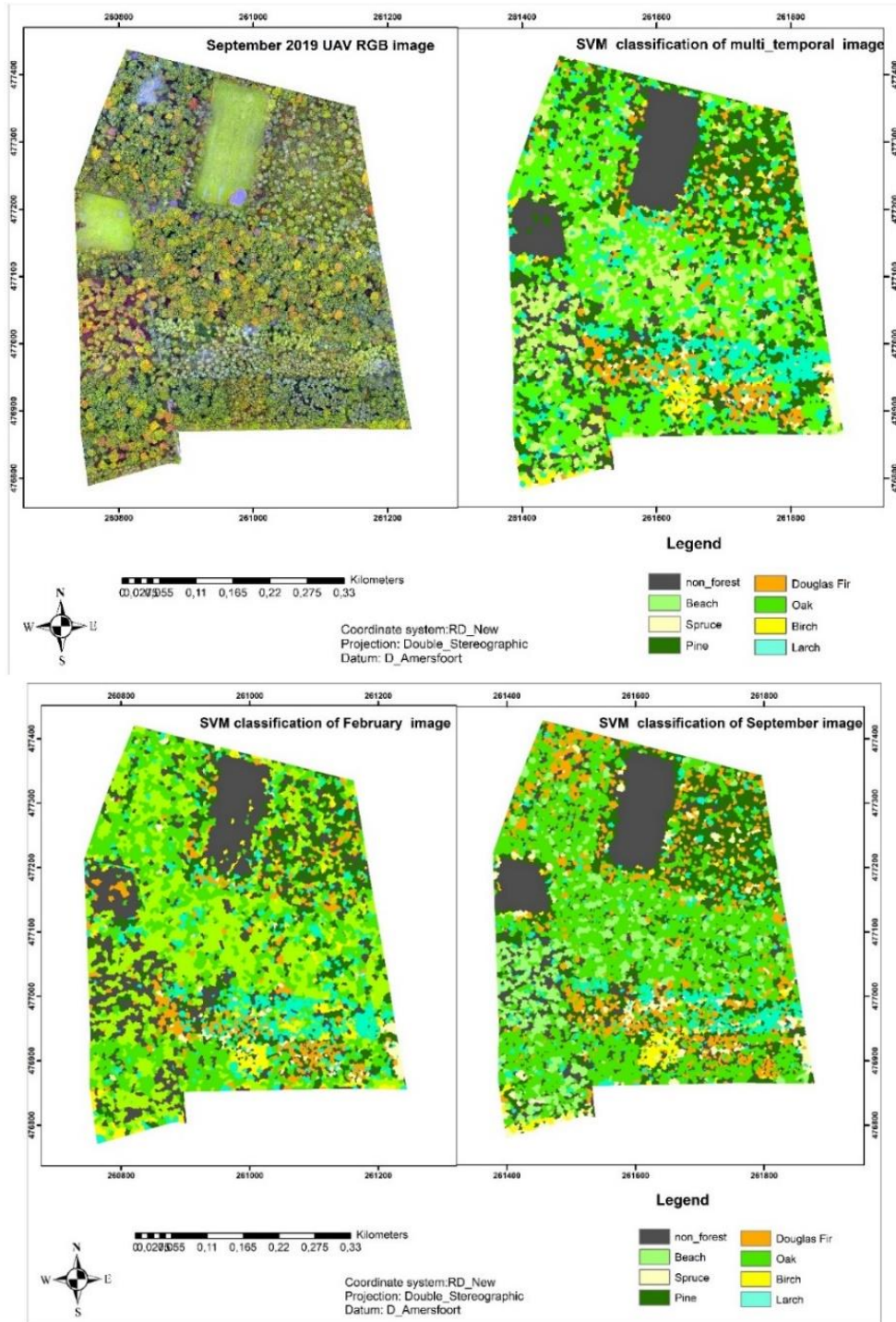

Figure 21: Spatial distribution of tree species classification using SVM classier for leaf-on, leaf-off and for the combination of leaf-on and leaf-off season UAV-RGB image.

5. DISCUSSION

5.1 Tree Crown delineation using Multi-resolution segmentation (MRS)

Image segmentation is a critical step in object-based image analysis (OBIA) as it affects the classification result considerably (Hossain & Chen, 2019). Finding the best combinations of segmentation parameters for MRS is a prerequisite to improve the segmentation result and to reduce the propagation error of segmentation into the classification result (Drǎguţ et al., 2014; Zhang et al., 2018). The best scale, shape and compactness parameters for mature and young forest stands were determined iteratively. The values of the corresponding parameters for mature forest stand are 150, 0.6 and 0.8, while for the young forest stand are 50, 0.6 and 0.6. Among these parameters, we found that scale is the most sensitive parameter which substantially affects the segmentation result, and this result is consistent with the findings of the previous studies (e.g., Cao et al., 2018; Drǎguţ et al., 2014; Ghosh & Joshi, 2014; Ming et al., 2015). We also found different segmentation parameters for the two forest stands. This discrepancy mainly associated with the difference in canopy coverage, forest structure and a difference in spectral properties of tree species.

The MRS proved to be an effective segmentation algorithm in the mature mixed forest stand as explained by the highest overall accuracy of 83% when a combination of Orthophoto and CHM used, and 82% when a single Orthophoto used. Similarly, MRS produced a good segmentation result in young mixed forest stand using a combination of CHM and Orthophoto (76%) and single Orthophoto (73%). The lower segmentation accuracy in the young forest may be attributed to the random distribution of mature deciduous and coniferous species which in turn affects the optimized scale parameters assigned for this forest stand. In addition, intermingled leaves and the small size of the crown may partly affect the accuracy of segmentation result as well. Multi-resolution segmentation produced the higher segmentation accuracy result in the mature forest stand than in the young forest stand. Moreover, a combination of UAV-derived CHM and Orthophoto slightly underestimates the tree crown segmentation of the mature forest stand but improves the young forest stand by 3%. This discrepancy may be associated with the accuracy of UAV derived CHM which is better in the young forest stand than in mature forest stand. The possible reason for the betterment of UAV derived CHM in young forest stand is that this forest stand may yield better DTM as compared to mature forest stand. In this study, note that, the DTM of the two forest stands were determined using the leaf-off season UAV-RGB image in which the broadleaved species, the dominant trees in the study area, drops their leaves in this season. However, a few number of coniferous species were observed in the young forest stand than in mature forest stand and this may partly contribute its parts to improve the accuracy of DTM in young forest stand as UAV derived DTM mainly depends very much on the canopy openness (Obeng-manu, 2019).

Compared to the previous studies who reported that tree height improves the segmentation accuracy in mixed forest stand (Guo et al., 2017; Sankey et al., 2018), we found inconsistent result. This discrepancy is mainly associated with the difference of the data source used by these studies to derive CHM. For example, Guo et al., (2017) used UAV born LiDAR data to derive CHM for forest mapping, and they found that the UAV born LiDAR system produced high accuracy of DTM. Similarly, Sankey et al., (2018) applied UAV LiDAR data for vegetation mapping, and they found that UAV LiDAR showed the highest accuracy in generating DTM as Lidar penetrate the canopy but UAV cannot. Moreover, LiDAR data is a measurement while UAV data is an output of the Orthophoto mosaic of many images in SFM process. This indicates that further improvement of UAV derived CHM would be necessary by integrating UAV data with LiDAR.

5.2. Comparison of machine learning algorithms

The best machine learning algorithms for classifying seven tree species in a mixed temperate forest would be characterized by high overall accuracy and high kappa coefficient. Taking this into account, the SVM outperformed RF and KNN classifiers (Table 8) and produced the highest overall accuracy and kappa coefficient in a mixed temperate forest. This result comparable with findings of Wessel et al. (2018): SVM showed the highest performance in separating broadleaved and coniferous tree species in a temperate forest, Germany. However, the accuracy of all the three classifiers considerably varied when we considered their performance in classifying four tree species from the coniferous and three species from the broadleaved tree types separately.

All the classifiers produced the lowest performance in separating the species within coniferous tree species group when compared to the broadleaved ones. This is mainly due to the fact that the coniferous tree species (4 in number) have similar spectral characteristics. Though the performance of these classifiers to separate tree species in temperate forests varies from region to region and from species to species (e.g. Cao et al., 2018; Modzelewska et al., 2020; Xie et al., 2019), we found that SVM is the best classifier in this study region as compared to RF and KNN. The low performance of random forest compared to SVM may be partly caused by the number of samples (training and test) used (Luan et al., 2020). As presented in Table 11, the overall accuracy of the SVM and KNN classifiers are less sensitive to sample size. In contrast, the RF classifier is highly sensitive to the number of samples which in turn affects its accuracy in classifying tree species. This result is consistent with the findings reported by Thanh et al. (2017) and Luan et al. (2020) who found that the accuracy of RF is increased as sample size increase. The RF may outperform all the remaining machine learning algorithm when the sample size is very large and thus, further studies could be needed to validate RF classifier by taking more than 247 samples. Overall, the sensitivity result obtained from this study is comparable with the findings of Qian et al. (2015) as well.

Table 11: Sensitivity of machine learning algorithms for different size of sample sizes.

Sample Size	SVM			RF			KNN	
	Cost	Gamma	Accuracy%	Ntree	Mtry	Accuracy %	K	Accuracy %
50	35	0.24	77.3	70	5	61.8	3	72.1
100	25	0.21	78.4	50	5	64.4	3	72.8
150	18	0.31	77.5	200	5	67.9	5	73.1
200	8	0.28	78.8	320	5	70.3	5	72.9
247	10	0.32	78.9	500	5	74.4	5	73.4

5.3. Seasonal effects on tree species classification

Tree species classification based on the combination of leaf-on and leaf-off season UAV-RGB images showed that dataset from the different seasons could improve the classification result, especially in a mixed temperate forest. This is mainly due to the fact that the combination of two UAV-RGB images take the advantage of tree species classification under the leaf-on and leaf-off conditions. Meaning, the leaf-on season improved the classification of the broadleaved species whereas the leaf-off season improves the coniferous species classification. These results are consistent with the findings of the previous studies who reported that leaf-on and leaf-off LiDAR images improved the broadleaved and coniferous tree species classification (Kim et al., 2009). Similarly, we also found comparable result with the findings of Wessel et al. (2018) and Persson et al. (2018) who classified these species using multi-temporal Sentinel image.

The leaf-off season (February) UAV-RGB image performs poorly to separate broadleaved tree species as the broadleaved species tend to drop their leaves in this season. The leaf-on season outperforms the leaf-off and the combination of leaf-on and leaf-off season in identifying broadleaved tree species but not for coniferous species. A good performance of the broadleaved tree species classification in the leaf-on season is mainly attributed to the dissimilarity of spectral reflectance of the trees species in this season. As can be shown in Figure 22, most of the broadleaved species exhibit higher variabilities of spectral reflectance in the leaf-on (September) season than in the leaf-off (February) season, and this factor makes the broadleaved tree species to be separated well. In contrast, all the coniferous species can be more separated in the leaf-off season than in the leaf-on season. The fact that the coniferous species tend to show higher variabilities of spectral signature in the leaf-off season than in the leaf-on season as explained below.

In general, the classifiers showed poor performance in separating Pine species that are highly confused with Douglas Fir. However, the leaf-off season gave better classification result for Pine species, which is mainly attributed to the highest variabilities of the spectral profile. For example, the digital number (DN) value of Pine (Douglas Fir) species on the red band is 75 (110) in the leaf-off and 130 (148) in the leaf-on season. Despite Larch is a coniferous species, it behaves like the broadleaved tree species which tends to drop its

needle leaves in winter and looks white in this season. As a result, the spectral reflectance of this specie is very high (220) which can easily be separated in the leaf-off season as compared to the remaining tree species. However, Larch species exhibit similar spectral characteristics with the coniferous species especially with Spruce species. Overall, the spectral variability of the coniferous species is very high in leaf-off season than in the leaf-on season. Moreover, the spectral bands alone cannot separate all the tress species accurately as explained by the spectral profile illustrated in Figure 22, which showed similar spectral characteristics. Therefore, it is very important to consider multiple features such as spectral, texture and tree height as input for the classification.
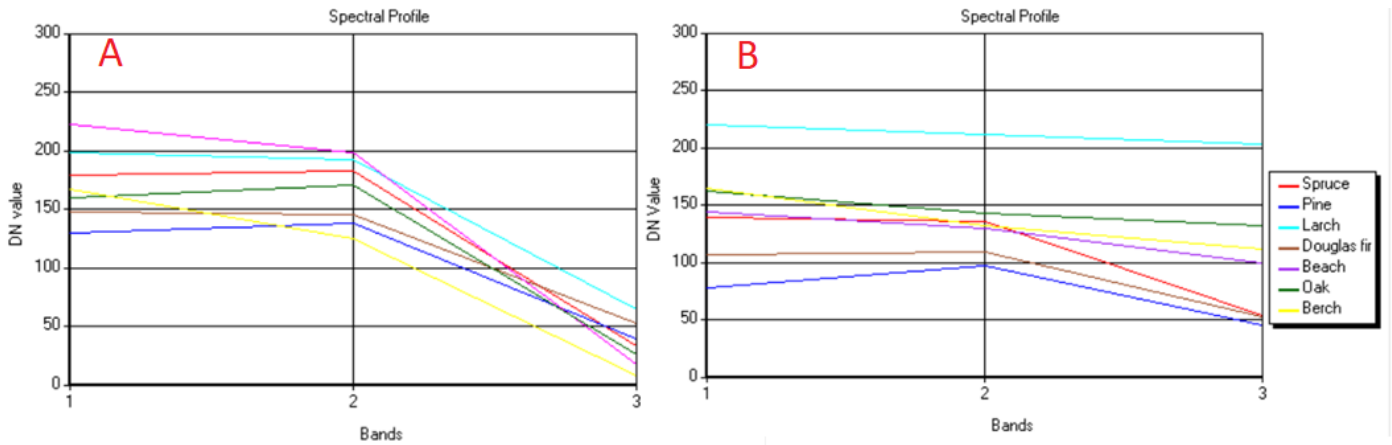
Figure 22: The average spectral reflectance curve of the tree species under the leaf-on (A) and leaf-off (B) conditions. Band 1, 2 and 3 refer Red, Green, and Blue. The first four species listed in the legend are coniferous species, and the remaining are the broadleaved ones.

Using a combination of two UAV-RGB images, we found a good tree species classification accuracy result in a mixed temperate forest, and we believe that this classification performance may be improved when we are using multispectral images that comprises the infrared and red edge bands (Deng et al., 2017). Moreover, despite efforts were made to consider additional UAV-RGB images captured in spring season for tree species classification, we did not perform the analysis as we obtained the spring season UAV-RGB image, Mid-May 2020, lately. However, based on our visual inspection assessment, the Orthophoto shown in Figure 23 may not improve the classification result as the tree species exhibit similar spectral characteristics, and most of them look like green. But still, there might be a chance to differentiate some of the tree species which have different shades of greenness which shows different spectral characteristics. This study suggests to use UAV-RGB image captured in the leaf-onset season (April but not May) UAV-RGB image which may improve the tree classification accuracy result.
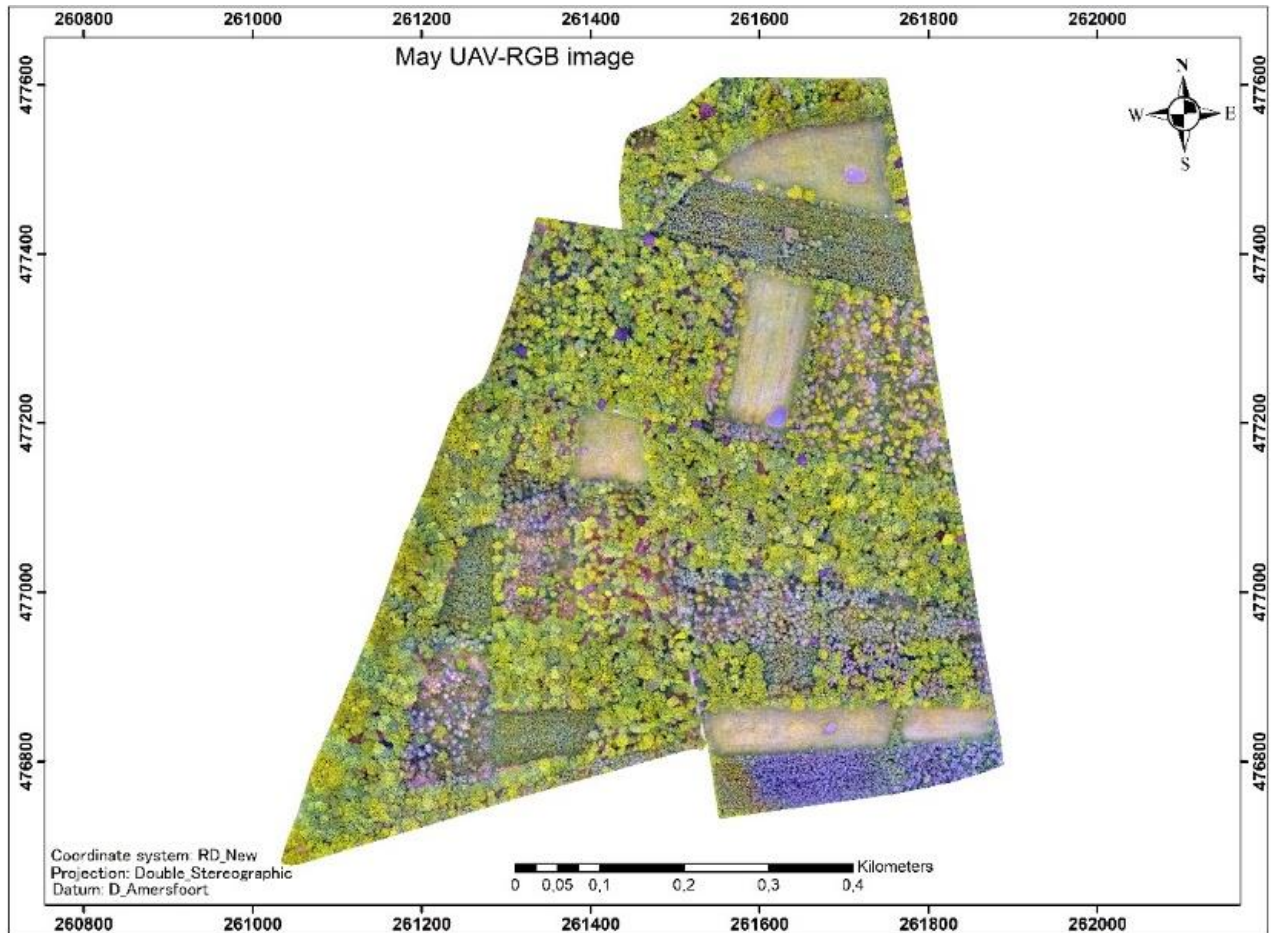
Figure 23: UAV-RGB image captured in May 2020

5.4. Implication for Natural Resource Management

The findings of this study are important to monitor Haagse Bos in a sustainable manner. This study suggests to use SVM classifier to classify tree species in a mixed temperate forest like Haagse Bos and has its own implication in estimating the above-ground biomass at the species level, in managing forest ecosystem, in assessing the biodiversity and ecosystem services, and in conserving endangered or critical tree species. Moreover, this tree species classification result would provide valuable information to natural resource managers to utilize/sell woods from the identified species.

6. CONCLUSION AND RECOMMENDATION

6.1.   CONCLUSION

This study aimed at classifying and mapping tree species using UAV-RGB images and machine learning algorithms in a mixed temperate forest, Haagse Bos Netherlands. For this purpose, the UAV-RGB images captured in September 2019 (leaf-on season) and February 2020 (leaf-off season) were used. A combination of leaf-on and leaf-off season UAV-RGB images were also applied to classify tree species. The object-based Support Vector Machine (SVM), K-nearest neighbour (KNN) and Random Forest (RF) classifiers were used to separate seven tree species, three from the broadleaved and four from the coniferous trees. The UAV-RGB image captured on the leaf-on season were used to compare all the three classifiers, and to assess the tree crown segmentation accuracy in the young and mature mixed forest stands using a single Orthophoto and combinations of canopy height model (CHM) and Orthophoto. The accuracy of the multi-resolution segmentation (MRS) algorithm in segmenting tree crown were assessed using three evaluation performance metrics: over segmentation, under segmentation and total segmentation error. Regarding the tree species classification, comparison of classifiers were made based on the overall accuracy and kappa coefficient, which were determined from the confusion matrix developed from the 5-fold cross validation. The best classifier was subsequently applied in the leaf-off and combinations of seasons of UAV-RGB images for classifying tree species.

Based on the findings of this study, the following conclusions can be drawn for each research question;
Question1: How accurately can the tree crowns be delineated by multi-resolution segmentation? Does a combination of Orthophoto and UAV derived CHM improves the segmentation accuracy result in mature and young forest stands?

- The MRS proved to be a powerful tool in segmenting the tree crown of the mature forest stand as explained by the highest overall accuracy of 83% when a combination of Orthophoto and CHM used, and 82% when a single Orthophoto used. MRS produced an overall accuracy of 76% and 73% segmentation accuracy in young forest stand when a combination of CHM and Orthophoto, and a single Orthophoto used, respectively. These indicate that we found a better segmentation result in mature forest stand than in young forest stand.
- The UAV-derived CHM improved the tree crown segmentation of young forest stand by 3% but it slightly reduced the segmentation accuracy of the mature forest stand by 1%. This discrepancy may partly be associated with the accuracy of UAV derived CHM.

Question2: Which classifiers (SVM, RF and KNN) perform best in differentiating tree species using September 2019 UAV-RGB image (leaf-on season)?

- Among the machine learning algorithms, using the leaf-on season UAV-RGB image, the SVM object-based classification produced the highest performance in classifying tree species with an overall accuracy and a kappa coefficient of 79% and 0.75, respectively.

- Results showed that the broadleaved tree species are better discriminated by RF whereas the KNN model produced the highest accuracy in classifying tree species categorized under coniferous species group. In general, the users can use RF classifier to classify the broadleaved tree species if they are interested to classify the broadleaved tree species alone. Similarly, they can use KNN for coniferous species classification. However, in a mixed temperate forest like Haagse Bos, we suggest to use SVM to classify tree species.

Question3: How accurate are tree classification results obtained from leaf-on and leaf-off season UAV-RGB images?

- The tree species classification under the leaf-off condition produced the lowest results as compared to the leaf-on season, and a combination of leaf-on and leaf-off season UAV-RGB image. However, coniferous tree species are best separated in the leaf-off season. In contrary, the broadleaved species are better differentiated in leaf-on season image.

Question4/5: Does the tree species classification accuracy result improve when the combinations of leaf-on and leaf-off season UAV-RGB images are used? Which UAV-RGB image (leaf-on, leaf-off, and/or combinations) yields best tree species classification result?

- The combination of leaf-on and leaf-off seasons UAV-RGB image, a combination of all bands (6) from different seasons, produced an overall accuracy of 83% and kappa coefficient of 0.75. This indicates that a combination of leaf-on and leaf-off seasons UAV-RGB image improves the classification accuracy result as compared to the classification result obtained from a single date UAV-RGB image. It improves the leaf-on and leaf-off season tree species classification by 3.7% and by 11.3 %, respectively.

6.2.   RECOMMENDATION

This study suggests to use SVM classifier in Haagse Bos to estimate the above-ground biomass at the species level and to manage endangered or critical species. Despite a combination of two UAV-RGB image produced a reasonable classification result (83%), further studies would be necessary to improve the classification accuracy result either using UAV multispectral or hyperspectral sensors or by incorporating additional UAV-RGB image captured in spring and summer seasons. It is important to acknowledge that the findings of this study may be limited by the number and distribution of training dataset used.

ANNEX

Annex1: Quality report for the February image

Summary

Project	last1
Processed	2020-04-06 01:32:04
Camera Model Name(s)	FC330_3.6_4000x3000 (RGB)
Average Ground Sampling Distance (GSD)	4.90 cm / 1.93 in
Area Covered	0.780 km^2 / 77.9534 ha / 0.30 sq. mi. / 192.7268 acres
Time for Initial Processing (without report)	54m:22s

Quality Check

? Images	median of 43490 keypoints per image	✓
? Dataset	767 out of 807 images calibrated (95%), all images enabled	✓
? Camera Optimization	0.02% relative difference between initial and optimized internal camera parameters	✓
? Matching	median of 1328.12 matches per calibrated image	✓
? Georeferencing	yes, 3 GCPs (3 3D), mean RMS error = 0.001 m	✓

? Preview
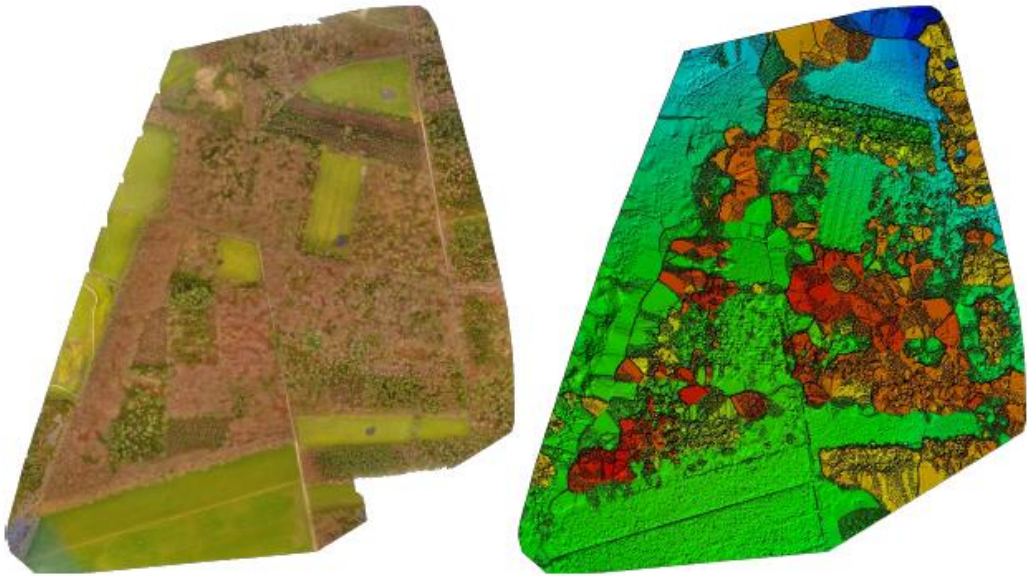
Figure 1: Orthomosaic and the corresponding sparse Digital Surface Model (DSM) before densification.

Annex 2: Feature extracted from February 2019 UAV-RGB image
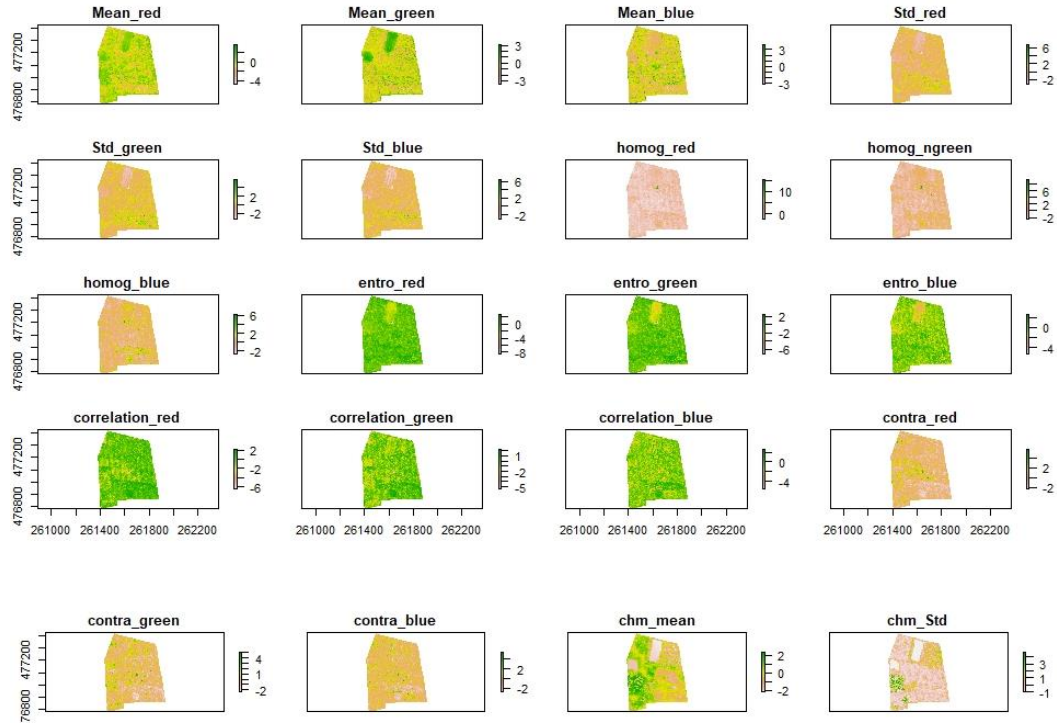
Annex 3: Feature extracted from the combination of two seasonal images
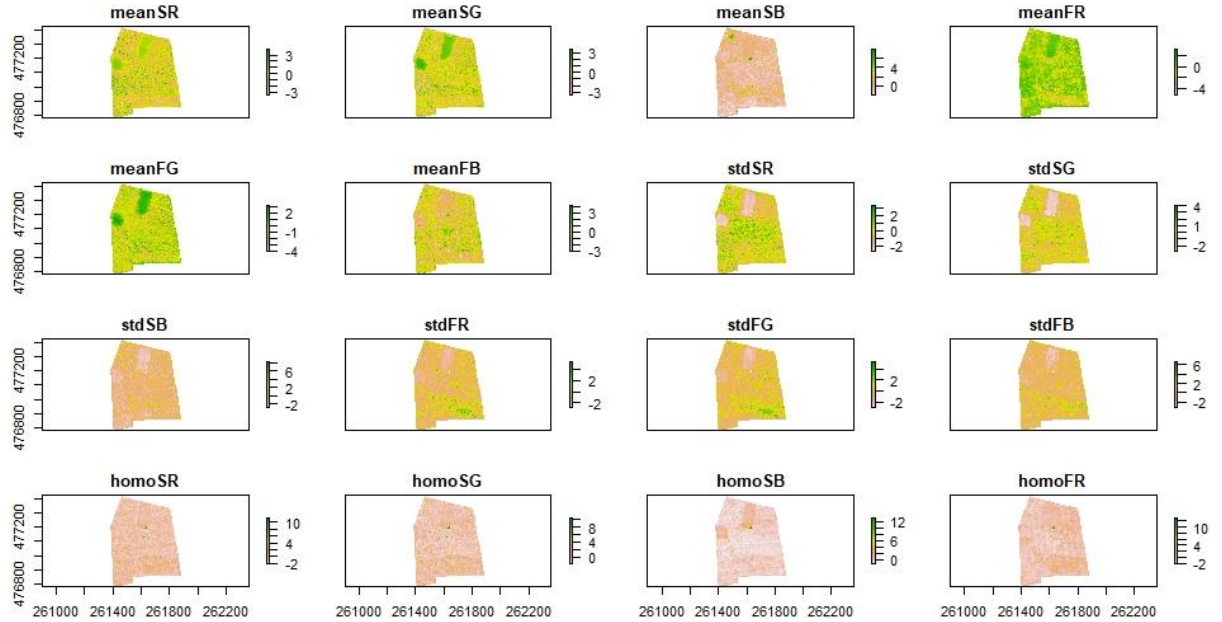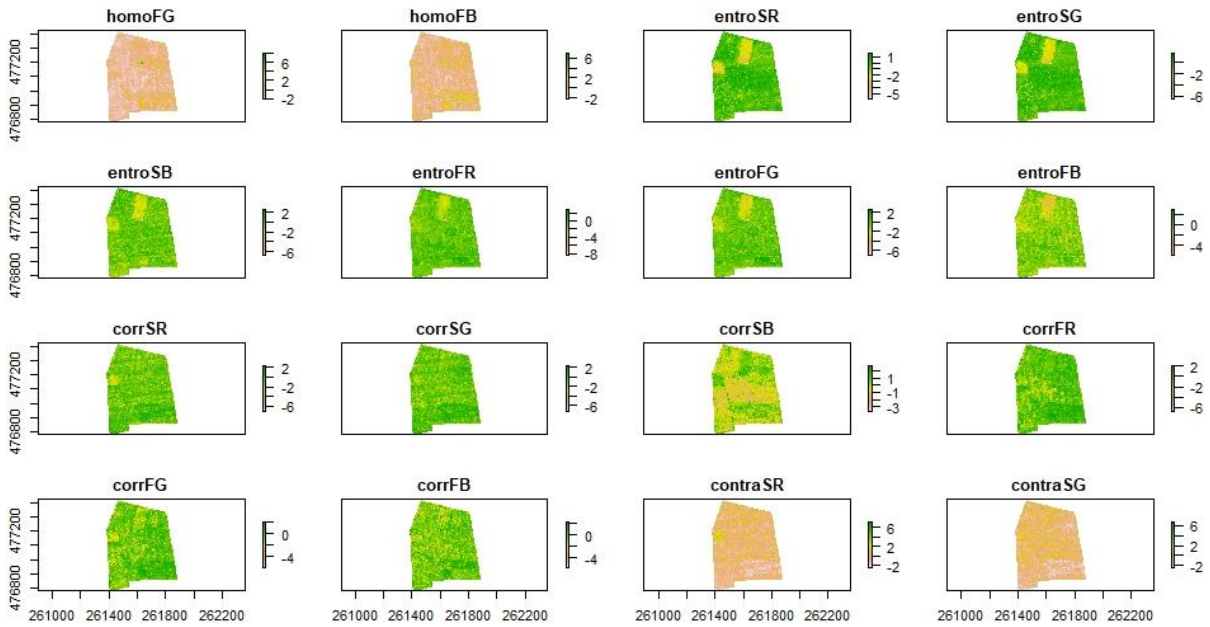
Annex 4: SVM code for classification

```
Path="E:/reserach/pix4d_new/Feb_data/sep+feb"
setwd(Path)
### SVM
setwd(Path)
files<-
c("meanSR.tif","meanSG.tif","meanSB.tif","meanFR.tif","meanFG.tif","meanFB.tif","stdSR.tif","stdSG.tif
","stdSB.tif","stdFR.tif","stdFG.tif","stdFB.tif","homoSR.tif","homoSG.tif","homoSB.tif","homoFR.tif","
homoFG.tif","homoFB.tif","entroSR.tif","entroSG.tif","entroSB.tif","entroFR.tif","entroFG.tif","entroF
B.tif","corrSR.tif","corrSG.tif","corrSB.tif","corrFR.tif","corrFG.tif","corrFB.tif","contraSR.tif","contraS
G.tif","contraSB.tif","contraFR.tif","contraFG.tif","contraFB.tif","stdCHM.tif","meanCHM.tif")
A<-stack(files)
A<-scale(A)
plot(A)
VTS <- readOGR(dsn=Path, layer="train3", stringsAsFactors = FALSE)
B<-data.frame(VTS@data,extract(A,VTS))
head(B)
selectfea<-c(3:40)

set.seed(100)
```

K-fold validation; splitting training and testing dataset

```
j <- kfold(B, k = 5, by=B$class)
table(j)
x <- list()
for (k in 1:5) {
  train <- B[j!= k, ]
  test <- B[j == k, ]
```

```
  SVM.lin.model <- svm(x=train[,selectfea],y=train$class,  type="C-classification", kernel = "radial", cost
=2.99 ,scale = TRUE)
  y=predict(SVM.lin.model,test[,selectfea])
  # create a data.frame using the reference and prediction
  x[[k]] <- cbind(test$class, as.integer(y))
}
y <- do.call(rbind, x)
y <- data.frame(y)
colnames(y) <- c('observed', 'predicted')
conmat <- table(y)
# number of cases
n <- sum(conmat)
n
##
# number of correctly classified cases per class
diag <- diag(conmat)
# Overall Accuracy
OA <- sum(diag) / n
OA


# observed (true) cases per class
rowsums <- apply(conmat, 1, sum)
p <- rowsums / n
# predicted cases per class
colsums <- apply(conmat, 2, sum)
q <- colsums / n
expAccuracy <- sum(p*q)
kappa <- (OA - expAccuracy) / (1 - expAccuracy)
kappa


###Producer and user accuracy  for SVM

# Producer accuracy
PA <- diag / colsums
# User accuracy
UA <- diag / rowsums
outAcc <- data.frame(producerAccuracy = PA, userAccuracy = UA)
outAcc
summary(SVM.lin.model)


##plotting and summary SVM classification
summary (SVM.lin.model)
SVMpred<-predict(A,SVM.lin.model)
writeRaster(SVMpred,filename="SVM_feb+sep.tif")
plot(SVMpred)
```

```
###Fine tuning of SVM radial model
OA <- sum(diag) / n
OA
C.vec=10^seq(0,3,len=20)
OA.vec=rep(0,20)
OAtr.vec=rep(0,20)
NSV=rep(0,20)

for (i in 1:length(C.vec)){
  SVM.lin.model <- svm(x=train[,selectfea], y=train$class,  type="C-classification", kernel = "radial", cost
= C.vec[i],gamma = 0.32, scale = TRUE)
  ypred=predict(SVM.lin.model, test[,selectfea])
  CM=table(prediction=ypred,truth=test$class)
  OA=sum(diag(CM))/length(test$class)
  print(OA)
  OA.vec[i]=OA

  ytr.pred=predict(SVM.lin.model, train[,selectfea])
  CM=table(prediction=ytr.pred,truth=train$class)
  OAtr=sum(diag(CM))/length(train$class)
  OAtr.vec[i]=OAtr
  NSV[i]=SVM.lin.model$tot.nSV
}

best.C=C.vec[which.max(OA.vec)]
best.C
SVM.lin.model <- svm(x=train[,selectfea], y=train$class,  type="C-classification", kernel = "radial", cost
= best.C, scale = TRUE)
ypred=predict(SVM.lin.model, test[,selectfea])
CM=table(prediction=ypred,truth=test$class)
OA=sum(diag(CM))/length(test$class)
OA
summary(SVM.lin.model)
###other ways to fine tune cost and gamma
x<-subset(B,select=-class)
y<-B$class
svm2<-tune(svm,train.x = x,train.y = y,kernel="radial",ranges = list(cost=10^(-1:2), gamma=c(0.5,1,2)),
        tunecontrol=tune.control(nrepeat = 5,sampling = "cross",cross = 5))
svm2
```

Annex 5 : KNN code used for classification

```
Path="E:/reserach/pix4d_new/Feb_data/sep+feb"
setwd(Path)
### KNN
setwd(Path)
files<-
c("meanSR.tif","meanSG.tif","meanSB.tif","meanFR.tif","meanFG.tif","meanFB.tif","stdSR.tif","stdSG.tif
```

```
","stdSB.tif","stdFR.tif","stdFG.tif","stdFB.tif","homoSR.tif","homoSG.tif","homoSB.tif","homoFR.tif","
homoFG.tif","homoFB.tif","entroSR.tif","entroSG.tif","entroSB.tif","entroFR.tif","entroFG.tif","entroF
B.tif","corrSR.tif","corrSG.tif","corrSB.tif","corrFR.tif","corrFG.tif","corrFB.tif","contraSR.tif","contraS
G.tif","contraSB.tif","contraFR.tif","contraFG.tif","contraFB.tif","stdCHM.tif","meanCHM.tif")
A<-stack(files)
A<-scale(A)
plot(A)
VTS <- readOGR(dsn=Path, layer="train3",  stringsAsFactors = FALSE)
B<-data.frame(VTS@data,extract(A,VTS))
head(B)
```
K-fold validation ;splitting training and testing dataset
```
j <- kfold(B, k = 5, by=B$class)
table(j)
x <- list()
for (k in 1:5) {
  train <- B[j!= k, ]
  test <- B[j == k, ]
  ctrl <- trainControl(method="repeatedcv",repeats = 3) #,classProbs=TRUE,summaryFunction =
twoClassSummary)
  knnFit <- train(class ~ ., data = train, method = "knn", trControl = ctrl,  tuneLength =
20,na.action="na.omit")

  y=predict(knnFit,test)
  # create a data.frame using the reference and prediction
  x[[k]] <- cbind(as.factor(test$class) , as.factor(y))
}
knnFit
plot(knnFit)

#accuracy assesement
y <- do.call(rbind, x)
y <- data.frame(y)
colnames(y) <- c('observed', 'predicted')
conmat <- table(y)
conmat
# number of cases
n <- sum(conmat)
n
##
# number of correctly classified cases per class
diag <- diag(conmat)
# Overall Accuracy
OA <- sum(diag) / n
OA

# observed (true) cases per class
```

```
rowsums <- apply(conmat, 1, sum)
p <- rowsums / n
# predicted cases per class
colsums <- apply(conmat, 2, sum)
q <- colsums / n
expAccuracy <- sum(p*q)
kappa <- (OA - expAccuracy) / (1 - expAccuracy)
kappa
###Producer and user accuracy for KNN
# Producer accuracy
PA <- diag / colsums
# User accuracy
UA <- diag / rowsums
outAcc <- data.frame(producerAccuracy = PA, userAccuracy = UA)
outAcc
KNN_predictt<-predict(A,knnFit)
writeRaster(KNN_predictt,filename="newf_knn.tif")
plot(KNN_predictt)
```

Annex 6: Random forest code applied in this study

```
rm(list=ls(all=TRUE))
require(rgdal)
require("e1071")
library(MASS)
require(kernlab)
library(dismo)
library(randomForest)
library(sp)
library(tcltk)
library(rasterVis)
library(class)
library(ISLR)
library(caret)
# Change this accoording to your data folder path
Path="E:/reserach/pix4d_new/Feb_data/sep+feb"
setwd(Path)
### randomforest
setwd(Path)
files<-
c("meanSR.tif","meanSG.tif","meanSB.tif","meanFR.tif","meanFG.tif","meanFB.tif","stdSR.tif","stdSG.tif
","stdSB.tif","stdFR.tif","stdFG.tif","stdFB.tif","homoSR.tif","homoSG.tif","homoSB.tif","homoFR.tif","
homoFG.tif","homoFB.tif","entroSR.tif","entroSG.tif","entroSB.tif","entroFR.tif","entroFG.tif","entroF
B.tif","corrSR.tif","corrSG.tif","corrSB.tif","corrFR.tif","corrFG.tif","corrFB.tif","contraSR.tif","contraS
G.tif","contraSB.tif","contraFR.tif","contraFG.tif","contraFB.tif","stdCHM.tif","meanCHM.tif")
A<-stack(files)
### random forest
A<-scale(A)
```

```r
plot(A)
VTS <- readOGR(dsn=Path, layer="train3",  stringsAsFactors = FALSE)
B<-data.frame(VTS@data,extract(A,VTS))
head(B)
selectfea<-c(3:40)
set.seed(500)
## K-fold validation ;splitting training and testing dataset
j <- kfold(B, k = 5, by=B$class)
table(j)
x <- list()
for (k in 1:5) {
  train <- B[j!= k, ]
  test <- B[j == k, ]
  rf.mdl<-randomForest(x=train[,selectfea],y=as.factor(train$class),ntree = 500, importance = TRUE,
              proximity = FALSE)
  y=predict(rf.mdl,test[,selectfea])
  # create a data.frame using the reference and prediction
  x[[k]] <- cbind(test$class, as.integer(y))
}
###plotting and variableimportance for RF
rf.mdl
varImpPlot(rf.mdl)
y<-predict(A,rf.mdl,filename="new_RF.tif",
type="response",na.rm=TRUE,progress="window",overwrite=TRUE)
plot(y)
writeRaster(y,filename="new_RF.tif")
par(xpd=FALSE)
plot(y,legend=FALSE,col=c("lightcyan3","royalblue","forestgreen","coral3"),
    xaxt="n",yaxt="n",main="RF Classification")
par(xpd=TRUE)
legend("bottom",legend=c("ki","abe","fu","me"),
    fill=c("lightcyan3","royalblue","forestgreen","coral3"),horiz = T,
    inset = 0.075)
y <- do.call(rbind, x)
y <- data.frame(y)
colnames(y) <- c('observed', 'predicted')
conmat <- table(y)
conmat
# number of cases
n <- sum(conmat)
n
##
# number of correctly classified cases per class
diag <- diag(conmat)
# Overall Accuracy
OA <- sum(diag) / n
```

OA

observed (true) cases per class

rowsums <- apply(conmat, 1, sum)

p <- rowsums / n

predicted cases per class

colsums <- apply(conmat, 2, sum)

q <- colsums / n

expAccuracy <- sum(p*q)

kappa <- (OA - expAccuracy) / (1 - expAccuracy)

kappa

###Producer and user accuracy for RF

Producer accuracy

PA <- diag / colsums

User accuracy

UA <- diag / rowsums

outAcc <- data.frame(producerAccuracy = PA, userAccuracy = UA)

outAcc

Annex7: RF confusion matrix

observed	predicted								total	UA
	NON_FOREST	BEECH	SPRUCE	PINE	FIR	OAK	BIRCH	LARCH		
NON_FORES	32	0	0	4	0	0	0	0	36	0.888889
BEECH	0	38	0	1	0	1	0	0	40	0.95
SPRUCE	2	0	6	1	2	4	2	1	18	0.333333
PINE	7	0	2	5	4	3	0	1	22	0.227273
FIR	0	1	2	1	32	3	0	2	41	0.780488
OAK	0	1	0	0	3	40	0	0	44	0.909091
BIRCH	1	0	0	0	0	1	15	0	17	0.882353
LARCH	0	0	1	1	5	6	0	16	29	0.551724
									184	247
								OA	0.744939	
TOTAL	42	40	11	13	46	58	17	20		
PA	0.761904762	0.95	0.545455	0.384615	0.695652	0.689655	0.882353	0.8		
								OAC	53.63	
								OAD	92.07	

Annex8: SVM confusion matrix

observed	predicted								total	UA
	NON_FOR	BEECH	SPRUSE	PINE	FIR	OAK	BIRCH	LARCH		
NON_FOR	34	0	0	2	0	0	0	0	36	0.944444
BEECH	1	38	0	1	0	0	0	0	40	0.95
SPRUSE	0	0	11	0	3	1	1	2	18	0.611111
PINE	8	0	1	7	2	3	0	1	22	0.318182
FIR	0	0	3	1	35	1	0	1	41	0.853659
OAK	0	0	0	1	3	38	0	2	44	0.863636
BIRCH	0	0	0	0	0	1	16	0	17	0.941176
LARCH	0	0	1	1	3	8	0	16	29	0.551724
									195	247
								OA	0.789474	
TOTAL	43	38	16	13	46	52	17	22		
PA	0.790698	1	0.6875	0.538462	0.76087	0.730769	0.941176	0.727273		
								OAC	62.72	
								OAD	91.08	

Annex9: KNN confusion matrix

	predicted								total	UA
observed	NON_FOREST	BEECH	SPRUCE	PINE	FIR	OAK	BIRCH	LARCH		
NON_FOREST	28	0	1	5	0	4	1	1	40	0.7
BEECH	0	14	0	0	0	2	0	1	17	0.823529
SPRUCE	0	0	34	3	0	1	1	2	41	0.829268
PINE	0	0	8	12	0	8	0	1	29	0.413793
FIR	0	0	0	0	33	1	2	0	36	0.916667
OAK	0	0	5	1	0	37	1	0	44	0.840909
BIRCH	0	1	4	0	6	4	5	2	22	0.227273
LARCH	1	2	1	0	0	2	0	12	18	0.666667
									175	247
								OA	0.708502	
TOTAL	29	17	53	21	39	59	10	19		
PA	0.965517241	0.823529	0.641509	0.571429	0.846154	0.627119	0.5	0.631579		
								OAC	73.38	
								OAD	67.46	

Annex 10: February image confusion matrix

	predicted								total	UA
observed	NON_FOREST	BEECH	SPRUCE	PINE	FIR	OAK	BIRCH	LARCH		
NON_FOREST	29	0	0	3	1	1	0	2	36	0.805556
BEECH	0	30	0	1	0	9	0	0	40	0.75
SPRUCE	1	0	8	0	7	1	1	0	18	0.444444
PINE	3	3	0	10	1	4	0	1	22	0.454545
FIR	2	1	3	1	33	0	0	1	41	0.804878
OAK	1	3	0	1	0	36	3	0	44	0.818182
BIRCH	0	2	0	0	0	4	10	1	17	0.588235
LARCH	0	2	1	0	1	3	2	20	29	0.689655
									176	247
								OA	0.712551	
TOTAL	36	41	12	16	43	58	16	25		
PA	0.805555556	0.731707	0.666667	0.625	0.767442	0.62069	0.625	0.8		
								OAC	64.54	
								OAD	75.24	

Annex11: Combination of the two seasonal images confusion matrix

	predicted								total	UA
observed	NON_FOREST	BEECH	SPRUCE	PINE	FIR	OAK	BIRCH	LARCH		
NON_FOREST	32	0	0	3	0	0	0	1	36	0.888889
BEECH	1	37	0	2	0	0	0	0	40	0.925
SPRUSE	0	1	12	0	5	0	0	0	18	0.666667
PINE	1	2	0	15	0	1	2	0	21	0.714286
FIR	0	0	0	0	39	1	0	2	42	0.928571
OAK	1	2	0	1	3	37	0	0	44	0.840909
BIRCH	1	0	0	0	0	0	15	1	17	0.882353
LARCH	0	1	1	0	1	8	1	17	29	0.586207
									204	247
								OA	0.825911	
TOTAL	36	43	13	21	48	47	18	21		
PA	0.888888889	0.860465	0.923077	0.714286	0.8125	0.787234	0.833333	0.809524		
								OAC	75.45	
								OAD	88.11	

Annex12: The area coverage of each tree species classfied by SVM classfier using leaf-on season UAV-RGB image

Species group	Classified tree species	Area coverage (Ha)
Coniferous	Douglas fir	2.62
	Pine	3.80
	Spruce	0.90
	Larch	1.40
Sub-Total		7.80
Broadleaved	Oak	6.33
	Beech	4.64
	Birch	0.50
Sub-Total		11.50
Non-tree		3.82
Total		23.95

REFERENCES

Barredo José, I., Bastrup-Birk, A., Teller, A., Onaindia, M., de Manuel Beatriz Fernández, Madariaga, I., … Schmullius, C. (2015). *Mapping and assessment of forest ecosystems and their services – Applications and guidance for decision making in the framework of MAES*. https://doi.org/10.2788/720519

Belgiu, M., & Drăgu, L. (2016). Random forest in remote sensing: A review of applications and future directions. *ISPRS Journal of Photogrammetry and Remote Sensing*, *114*, 24–31. https://doi.org/10.1016/j.isprsjprs.2016.01.011

Blaschke, T., Lang, S., & Hay, G. J. (2008). Preface. *Object-Based Image Analysis: Spatial Concepts for Knowledge-Driven Remote Sensing Applications*, (January 2008), V–VIII. https://doi.org/10.1007/978-3-540-77058-9

Bonan, G. B. (2008). Forests and climate change: Forcings, feedbacks, and the climate benefits of forests. *Science*, *320*(5882), 1444–1449. https://doi.org/10.1126/science.1155121

Breiman, L. (2001). Random Forests. transparencias. *Statistics*, *45*(1), 1–33. https://doi.org/10.1023/A:1010933404324

Brovkina, O., Cienciala, E., Surový, P., & Janata, P. (2018). Unmanned aerial vehicles (UAV) for assessment of qualitative classification of Norway spruce in temperate forest stands. *Geo-Spatial Information Science*, *21*(1), 12–20. https://doi.org/10.1080/10095020.2017.1416994

Bruzzone, L., & Persello, C. (2009). Approaches based on support vector machine to classification of remote sensing data. *Handbook of Pattern Recognition and Computer Vision, Fourth Edition*, 329–352. https://doi.org/10.1142/9789814273398_014

Cao, J., Leng, W., Liu, K., Liu, L., He, Z., & Zhu, Y. (2018a). Object-Based mangrove species classification using unmanned aerial vehicle hyperspectral images and digital surface models. *Remote Sensing*, *10*(1). https://doi.org/10.3390/rs10010089

Cao, J., Leng, W., Liu, K., Liu, L., He, Z., & Zhu, Y. (2018b). Object-Based Mangrove Species Classification Using Unmanned Aerial Vehicle Hyperspectral Images and Digital Surface Models. *Remote Sensing*, *10*(2), 89. https://doi.org/10.3390/rs10010089

Chen, J., Li, J., Pan, D., Zhu, Q., & Mao, Z. (2012). Edge-guided multiscale segmentation of satellite multispectral imagery. *IEEE Transactions on Geoscience and Remote Sensing*, *50*(11 PART1), 4513–4520. https://doi.org/10.1109/TGRS.2012.2194502

Clinton, N., Holt, A., Scarborough, J., Yan, L. I., & Gong, P. (2010). Accuracy assessment measures for object-based image segmentation goodness. *Photogrammetric Engineering and Remote Sensing*, *76*(3), 289–299. https://doi.org/10.14358/PERS.76.3.289

Delpierre, N., Vitasse, Y., Chuine, I., Guillemot, J., Bazot, S., Rutishauser, T., & Rathgeber, C. B. K. (2016). Temperate and boreal forest tree phenology: from organ-scale processes to terrestrial ecosystem models. *Annals of Forest Science*, *73*(1), 5–25. https://doi.org/10.1007/s13595-015-0477-6

Deng, S., Katoh, M., Takenaka, Y., Cheung, K., Ishii, A., Fujii, N., & Gao, T. (2017). Tree species classification of broadleaved forests in Nagano, central Japan, using airborne laser data and multispectral images. *International Archives of the Photogrammetry, Remote Sensing and Spatial Information Sciences - ISPRS Archives*, *42*(3W3), 33–38. https://doi.org/10.5194/isprs-archives-XLII-3-W3-33-2017

Dra, L. (2010). ESP : A tool to estimate scale parameter for multiresolution image segmentation of remotely sensed data ESP : a tool to estimate scale parameter for multiresolution image segmentation of remotely sensed data ˘ gut, (June). https://doi.org/10.1080/13658810903174803

Drǎguţ, L., Csillik, O., Eisank, C., & Tiede, D. (2014). Automated parameterisation for multi-scale image segmentation on multiple layers. *ISPRS Journal of Photogrammetry and Remote Sensing*, *88*, 119–127. https://doi.org/10.1016/j.isprsjprs.2013.11.018

Duro, D. C., Franklin, S. E., & Dubé, M. G. (2012). A comparison of pixel-based and object-based image analysis with selected machine learning algorithms for the classification of agricultural landscapes using SPOT-5 HRG imagery. *Remote Sensing of Environment*, *118*, 259–272. https://doi.org/10.1016/j.rse.2011.11.020

Effiom, A. E., van Leeuwen, L. M., Nyktas, P., Okojie, J. A., & Erdbrügger, J. (2019). Combining unmanned aerial vehicle and multispectral Pleiades data for tree species identification, a prerequisite for accurate carbon estimation. *Journal of Applied Remote Sensing*, *13*(03), 1. https://doi.org/10.1117/1.jrs.13.034530

Esch, T., Thiel, M., Bock, M., Roth, A., & Dech, S. (2008). Improvement of image segmentation accuracy based on multiscale optimization procedure. *IEEE Geoscience and Remote Sensing Letters*, *5*(3), 463–467. https://doi.org/10.1109/LGRS.2008.919622

Eurostat. (2018). Retrieved June 7, 2020, from https://ec.europa.eu/eurostat/web/products-eurostat-news/-/EDN-20180321-1

Fan, J., Yau, D. K. Y., Elmagarmid, A. K., & Aref, W. G. (2001). Automatic image segmentation by integrating color-edge extraction and seeded region growing. *IEEE Transactions on Image Processing*, *10*(10), 1454–1466. https://doi.org/10.1109/83.951532

Feng, X., & Li, P. (2019). A tree species mapping method from UAV images over urban area using similarity in tree-crown object histograms. *Remote Sensing*, *11*(17). https://doi.org/10.3390/rs11171982

Fischler, M. A., & Bolles, R. C. (1981). RANSAC1981.pdf. *Graphics and Image Processing*, *24*(6), 381–395. https://doi.org/10.1145/358669.358692

Ghosh, A., & Joshi, P. K. (2014). A comparison of selected classification algorithms for mappingbamboo patches in lower Gangetic plains using very high resolution WorldView 2 imagery. *International Journal of Applied Earth Observation and Geoinformation*, *26*(1), 298–311. https://doi.org/10.1016/j.jag.2013.08.011

GitHub - artifabrian/dynamic-knn-gpu: Dynamic k-Nearest Neighbours using TensorFlow with GPU

support! (n.d.). Retrieved April 10, 2020, from https://github.com/artifabrian/dynamic-knn-gpu

Grabska, E., Hostert, P., Pflugmacher, D., & Ostapowicz, K. (2019). Forest stand species mapping using
the sentinel-2 time series. *Remote Sensing*, *11*(10), 1–24. https://doi.org/10.3390/rs11101197

Gu, H., Han, Y., Yang, Y., Li, H., Liu, Z., Soergel, U., … Cui, S. (2018). An efficient parallel multi-scale
segmentation method for remote sensing imagery. *Remote Sensing*, *10*(4), 1–18.
https://doi.org/10.3390/rs10040590

Guo, Q., Su, Y., Hu, T., Zhao, X., Wu, F., Li, Y., … Wang, X. (2017). An integrated UAV-borne lidar
system for 3D habitat mapping in three forest ecosystems across China. *International Journal of Remote
Sensing*, *38*(8–10), 2954–2972. https://doi.org/10.1080/01431161.2017.1285083

Haralick, R. M., Dinstein, I., & Shanmugam, K. (1973). Textural Features for Image Classification. *IEEE
Transactions on Systems, Man and Cybernetics*, *SMC-3*(6), 610–621.
https://doi.org/10.1109/TSMC.1973.4309314

Heinzel, J., & Koch, B. (2012). Investigating multiple data sources for tree species classification in
temperate forest and use for single tree delineation. *International Journal of Applied Earth Observation and
Geoinformation*, *18*(1), 101–110. https://doi.org/10.1016/j.jag.2012.01.025

Hill, R. A., Wilson, A. K., George, M., & Hinsley, S. A. (2010). Mapping tree species in temperate
deciduous woodland using time-series multi-spectral data. *Applied Vegetation Science*, *13*(1), 86–99.
https://doi.org/10.1111/j.1654-109X.2009.01053.x

Hossain, M. D., & Chen, D. (2019). Segmentation for Object-Based Image Analysis (OBIA): A review of
algorithms and challenges from remote sensing perspective. *ISPRS Journal of Photogrammetry and
Remote Sensing*, *150*(November 2018), 115–134. https://doi.org/10.1016/j.isprsjprs.2019.02.009

Hsu, C.-W. (2010). A Practical Guide to Support Vector Classification. *Theory, Culture and Society*, *17*(1), 39–
61. https://doi.org/10.1177/02632760022050997

Hu, B. (2012). Exploring high-density airborne light detection and ranging data for classification of mature
coniferous and deciduous trees in complex Canadian forests. *Journal of Applied Remote Sensing*, *6*(1),
063536. https://doi.org/10.1117/1.jrs.6.063536

Jakubowski, M. K., Li, W., Guo, Q., & Kelly, M. (2013). Delineating individual trees from lidar data: A
comparison of vector- and raster-based segmentation approaches. *Remote Sensing*, *5*(9), 4163–4186.
https://doi.org/10.3390/rs5094163

Kamal, M., & Phinn, S. (2011). Hyperspectral data for mangrove species mapping: A comparison of pixel-
based and object-based approach. *Remote Sensing*, *3*(10), 2222–2242.
https://doi.org/10.3390/rs3102222

Kim, S., McGaughey, R. J., Andersen, H. E., & Schreuder, G. (2009). Tree species differentiation using
intensity data derived from leaf-on and leaf-off airborne laser scanner data. *Remote Sensing of
Environment*, *113*(8), 1575–1586. https://doi.org/10.1016/j.rse.2009.03.017

Kovacs, J. M., de Santiago, F. F., Bastien, J., & Lafrance, P. (2010). An Assessment of Mangroves in
Guinea, West Africa, Using a Field and Remote Sensing Based Approach. *Wetlands*, *30*(4), 773–782.

https://doi.org/10.1007/s13157-010-0065-3

Li, H., Gu, J. D., & Sun, H. (2008). Structure, topology and assembly of a 32-mer peptide corresponding to the loop 3 and transmembrane domain 4 of divalent metal transporter (DMT1) in membrane-mimetic environments. *Journal of Inorganic Biochemistry*, *102*(5–6), 1257–1266. https://doi.org/10.1016/j.jinorgbio.2007.12.019

Liarokapis, M. V., Artemiadis, P. K., & Kyriakopoulos, K. J. (2013). Task discrimination from myoelectric activity: A learning scheme for EMG-based interfaces. *IEEE International Conference on Rehabilitation Robotics*, (October). https://doi.org/10.1109/ICORR.2013.6650366

Lim, J., Kim, K. M., & Jin, R. (2019). Tree species classification using hyperion and sentinel-2 data with machine learning in South Korea and China. *ISPRS International Journal of Geo-Information*, *8*(3). https://doi.org/10.3390/ijgi8030150

Lin, Hsuan-Tien; Lin, C.-J. (2005). A study on sigmoid kernels for svm and the training of non-psd. *Http://Www.Csie.Ntu.Edu.Tw/~Cjlin/Papers/Tanh.Pdf*, 1–32. https://doi.org/20060927122853789664

Liu, K., Liu, L., Liu, H., Li, X., & Wang, S. (2014). Exploring the effects of biophysical parameters on the spatial pattern of rare cold damage to mangrove forests. *Remote Sensing of Environment*, *150*, 20–33. https://doi.org/10.1016/j.rse.2014.04.019

Lu, D., Li, G., Moran, E., Dutra, L., & Batistella, M. (2014). The roles of textural images in improving land-cover classification in the Brazilian Amazon. *International Journal of Remote Sensing*, *35*(24), 8188–8207. https://doi.org/10.1080/01431161.2014.980920

Lu, Y., & Jain, R. C. (1989). Behavior of Edges in Scale Space. *IEEE Transactions on Pattern Analysis and Machine Intelligence*, *11*(4), 337–356. https://doi.org/10.1109/34.19032

Luan, J., Zhang, C., Xu, B., Xue, Y., & Ren, Y. (2020). The predictive performances of random forest models with limited sample size and different species traits. *Fisheries Research*, *227*(February), 105534. https://doi.org/10.1016/j.fishres.2020.105534

Madonsela, S., Cho, M. A., Mathieu, R., Mutanga, O., Ramoelo, A., Kaszta, Ż., … Wolff, E. (2017). Multi-phenology WorldView-2 imagery improves remote sensing of savannah tree species. *International Journal of Applied Earth Observation and Geoinformation*, *58*(June), 65–73. https://doi.org/10.1016/j.jag.2017.01.018

Ming, D., Li, J., Wang, J., & Zhang, M. (2015). Scale parameter selection by spatial statistics for GeOBIA: Using mean-shift based multi-scale segmentation as an example. *ISPRS Journal of Photogrammetry and Remote Sensing*, *106*, 28–41. https://doi.org/10.1016/j.isprsjprs.2015.04.010

Modzelewska, A., Fassnacht, F. E., & Stereńczak, K. (2020). Tree species identification within an extensive forest area with diverse management regimes using airborne hyperspectral data. *International Journal of Applied Earth Observation and Geoinformation*, *84*(August 2019), 101960. https://doi.org/10.1016/j.jag.2019.101960

Mountrakis, G., Im, J., & Ogole, C. (2011). Support vector machines in remote sensing: A review. *ISPRS*

Journal of Photogrammetry and Remote Sensing, *66*(3), 247–259.
https://doi.org/10.1016/j.isprsjprs.2010.11.001

Myint, S. W., Gober, P., Brazel, A., Grossman-Clarke, S., & Weng, Q. (2011). Per-pixel vs. object-based
classification of urban land cover extraction using high spatial resolution imagery. *Remote Sensing of
Environment*, *115*(5), 1145–1161. https://doi.org/10.1016/j.rse.2010.12.017

Natesan, S., Armenakis, C., & Vepakomma, U. (2019). Resnet-based tree species classification using uav
images. *International Archives of the Photogrammetry, Remote Sensing and Spatial Information Sciences - ISPRS
Archives*, *42*(2/W13), 475–481. https://doi.org/10.5194/isprs-archives-XLII-2-W13-475-2019

Obeng-manu, C. (2019). *Assessing the accuracy of UAV-DTM generated under different forest canopy density and its
effect on estimation of aboveground carbon in Asubima forest, Ghana*. Retrieved from
https://library.itc.utwente.nl/papers_2019/msc/nrm/obeng-manu.pdf

Ohta, Y.-I., Kanade, T., & Sakai, T. (1980). Color information for region segmentation. *Computer Graphics
and Image Processing*, *13*(3), 222–241. https://doi.org/https://doi.org/10.1016/0146-664X(80)90047-7

Otero, V., Van De Kerchove, R., Satyanarayana, B., Martínez-Espinosa, C., Fisol, M. A. Bin, Ibrahim, M.
R. Bin, … Dahdouh-Guebas, F. (2018). Managing mangrove forests from the sky: Forest inventory
using field data and Unmanned Aerial Vehicle (UAV) imagery in the Matang Mangrove Forest
Reserve, peninsular Malaysia. *Forest Ecology and Management*, *411*(December 2017), 35–45.
https://doi.org/10.1016/j.foreco.2017.12.049

Pal, S. K., & Pal, N. R. (1987). Segmentation Based on Measures of Contrast, Homogeneity, and Region
Size. *IEEE Transactions on Systems, Man and Cybernetics*, *SMC-17*(5), 857–868.
https://doi.org/10.1109/TSMC.1987.6499294

Persson, M., Lindberg, E., & Reese, H. (2018). Tree species classification with multi-temporal Sentinel-2
data. *Remote Sensing*, *10*(11), 1–17. https://doi.org/10.3390/rs10111794

Platt, R. V., & Rapoza, L. (2008). An evaluation of an object-oriented paradigm for land use/land cover
classification. *Professional Geographer*, *60*(1), 87–100. https://doi.org/10.1080/00330120701724152

Pong, T. C., Shapiro, L. G., Watson, L. T., & Haralick, R. M. (1984). Experiments in segmentation using a
facet model region grower. *Computer Vision, Graphics and Image Processing*, *25*(1), 1–23.
https://doi.org/10.1016/0734-189X(84)90046-X

Qian, Y., Zhou, W., Yan, J., Li, W., & Han, L. (2015). Comparing Machine Learning Classifiers for
Object-Based Land Cover Classification Using Very High Resolution Imagery, 153–168.
https://doi.org/10.3390/rs70100153

Saba, F., Valadan Zoej, M. J., & Mokhtarzade, M. (2016). Optimization of Multiresolution Segmentation
for Object-Oriented Road Detection from High-Resolution Images. *Canadian Journal of Remote
Sensing*, *42*(2), 75–84. https://doi.org/10.1080/07038992.2016.1160770

Sankey, T. T., McVay, J., Swetnam, T. L., McClaran, M. P., Heilman, P., & Nichols, M. (2018). UAV
hyperspectral and lidar data and their fusion for arid and semi-arid land vegetation monitoring.
Remote Sensing in Ecology and Conservation, *4*(1), 20–33. https://doi.org/10.1002/rse2.44

Su, T., & Zhang, S. (2017). Local and global evaluation for remote sensing image segmentation. *ISPRS Journal of Photogrammetry and Remote Sensing*, *130*, 256–276. https://doi.org/10.1016/j.isprsjprs.2017.06.003

Thanh Noi, P., & Kappas, M. (2017). Comparison of Random Forest, k-Nearest Neighbor, and Support Vector Machine Classifiers for Land Cover Classification Using Sentinel-2 Imagery. *Sensors*, *18*(2), 18. https://doi.org/10.3390/s18010018

Thomas, N., Bunting, P., Lucas, R., Hardy, A., Rosenqvist, A., & Fatoyinbo, T. (2018). Mapping mangrove extent and change: A globally applicable approach. *Remote Sensing*, *10*(9), 1–20. https://doi.org/10.3390/rs10091466

Towards Data Science. (n.d.). Retrieved April 10, 2020, from https://towardsdatascience.com/

Viennois, G., Proisy, C., Feret, J.-B., Prosperi, J., Sidik, F., Suhardjono,Gaspar, P. (2016). Multitemporal Analysis of High-Spatial-Resolution Optical Satellite Imagery for Mangrove Species Mapping in Bali, Indonesia. *IEEE Journal of Selected Topics in Applied Earth Observations and Remote Sensing*, *9*(8), 3680–3686. https://doi.org/10.1109/JSTARS.2016.2553170

Wang, D., Wan, B., Qiu, P., Su, Y., Guo, Q., & Wu, X. (2018). Artificial mangrove species mapping using Pléiades-1: An evaluation of pixel-based and object-based classifications with selected machine learning algorithms. *Remote Sensing*, *10*(2),294. https://doi.org/10.3390/rs10020294

Wessel, M., Brandmeier, M., & Tiede, D. (2018). Evaluation of different machine learning algorithms for scalable classification of tree types and tree species based on Sentinel-2 data. *Remote Sensing*, *10*(9), 1419. https://doi.org/10.3390/rs10091419

Wietecha, M., Jelowicki, Ł., Mitelsztedt, K., Miścicki, S., & Stereńczak, K. (2019). The capability of species-related forest stand characteristics determination with the use of hyperspectral data. *Remote Sensing of Environment*, *231*(July), 111232. https://doi.org/10.1016/j.rse.2019.111232

Xie, Z., Chen, Y., Lu, D., Li, G., & Chen, E. (2019). Classification of land cover, forest, and tree species classes with Ziyuan-3 multispectral and stereo data. *Remote Sensing*, *11*(2), 1–27. https://doi.org/10.3390/rs11020164

Yan, G., Mas, J. F., Maathuis, B. H. P., Xiangmin, Z., & Van Dijk, P. M. (2006). Comparison of pixel-based and object-oriented image classification approaches - A case study in a coal fire area, Wuda, Inner Mongolia, China. *International Journal of Remote Sensing*, *27*(18), 4039–4055. https://doi.org/10.1080/01431160600702632

Yu, Q., Yu, Q., Gong, P., Clinton, N., Biging, G., Kelly, M., & Schirokauer, D. (2006). Objectbased detailed vegetation classification with airborne high spatial resolution remote sensing imagery. Photogrammetric Engineering and Remote. *Sensing*, *72*(7), 799–811. Retrieved from http://citeseerx.ist.psu.edu/viewdoc/summary?doi=10.1.1.211.3508

Zhang, Hongsheng, Wang, T., Liu, M., Jia, M., Lin, H., Chu, L. M., & Devlin, A. T. (2018). Potential of combining optical and dual polarimetric SAR data for improving mangrove species discrimination Using Rotation Forest. *Remote Sensing*, *10*(3),467. https://doi.org/10.3390/rs10030467

Zhang, Hui, Fritts, J. E., & Goldman, S. A. (2008). Image segmentation evaluation: A survey of unsupervised methods. *Computer Vision and Image Understanding*, *110*(2), 260–280. https://doi.org/10.1016/j.cviu.2007.08.003

Zhou, Y. T., Venkateswar, V., & Chellappa, R. (1989). Edge Detection and Linear Feature Extraction Using a 2-D Random Field Model. *IEEE Transactions on Pattern Analysis and Machine Intelligence*, *11*(1), 84–95. https://doi.org/10.1109/34.23115